Bioactive Materials 15 (2022) 409–425

Contents lists available at ScienceDirect

Bioactive Materials

journal homepage: www.keaipublishing.com/en/journals/bioactive-materials

Biocompatible reduced graphene oxide stimulated BMSCs induce acceleration of bone remodeling and orthodontic tooth movement through promotion on osteoclastogenesis and angiogenesis

Delong Jiao [a], Jing Wang [b], Wenting Yu [b], Ke Zhang [b], Ning Zhang [b], Lingyan Cao [c], Xinquan Jiang [c,**], Yuxing Bai [b,*]

[a] Institute of Dental Research, Beijing Stomatological Hospital & School of Stomatology, Capital Medical University, Beijing, 100050, China
[b] Department of Orthodontics, Beijing Stomatological Hospital & School of Stomatology, Capital Medical University, Beijing, 100050, China
[c] Department of Prosthodontics, Shanghai Ninth People's Hospital, Shanghai Jiao Tong University School of Medicine; College of Stomatology, Shanghai Jiao Tong University; National Center for Stomatology; National Clinical Research Center for Oral Diseases; Shanghai Key Laboratory of Stomatology; Shanghai Engineering Research Center of Advanced Dental Technology and Materials, Shanghai, 200011, China

ARTICLE INFO

Keywords:
Bone remodeling
Reduced graphene oxide
Angiogenesis
Osteoclastogenesis
Orthodontic tooth movement

ABSTRACT

We has synthesized the biocompatible gelatin reduced graphene oxide (GOG) in previous research, and in this study we would further evaluate its effects on bone remodeling in the aspects of osteoclastogenesis and angiogenesis so as to verify its impact on accelerating orthodontic tooth movement. The mouse orthodontic tooth movement (OTM) model tests *in vivo* showed that the tooth movement was accelerated in the GOG local injection group with more osteoclastic bone resorption and neovascularization compared with the PBS injection group. The analysis on the degradation of GOG in bone marrow stromal stem cells (BMSCs) illustrated its good biocompatibility *in vitro* and the accumulation of GOG in spleen after local injection of GOG around the teeth in OTM model *in vivo* also didn't influence the survival and life of animals. The co-culture of BMSCs with hematopoietic stem cells (HSCs) or human umbilical vein endothelial cells (HUVECs) in transwell chamber systems were constructed to test the effects of GOG stimulated BMSCs on osteoclastogenesis and angiogenesis *in vitro*. With the GOG stimulated BMSCs co-culture in upper chamber of transwell, the HSCs in lower chamber manifested the enhanced osteoclastogenesis. Meanwhile, the co-culture of GOG stimulated BMSCs with HUVECs showed a promotive effect on the angiogenic ability of HUVECs. The mechanism analysis on the biofunctions of the GOG stimulated BMSCs illustrated the important regulatory effects of PERK pathway on osteoclastogenesis and angiogenesis. All the results showed the biosecurity of GOG and the biological functions of GOG stimulated BMSCs in accelerating bone remodeling and tooth movement.

1. Introduction

Orthodontics has made great progress in clinical and technical aspects, which makes it possible to obtain satisfactory therapeutic effects. The applications of digital diagnosis and treatment stimulation system make the clinical operation more convenient and efficient, but the underlying physiological basis of orthodontic treatment hasn't been changed, which would not shorten the orthodontic treatment course significantly. In the current treatment techniques available in our clinic, the less destructive corticotomy surgery has replaced osteotomy as the preferred scheme to accelerate tooth movement for shortening treatment course [1]. The procedure is just involved with the perforation of the bone cortex and non-intrusion into the medulla, which arouses the regional acceleratory phenomenon (RAP) with active demineralization and re-mineralization of alveolar bone resulting in the increased bone remodeling [2]. Similar with the histological observation in cortical incision surgery, other researches on the nonsurgical interventions such as resonance vibration [3], laser irradiation [4], continuous injection of PTH [5], pulsed electromagnetic fields [6] and electric currents [7], also showed that these methods could accelerate orthodontic tooth

Peer review under responsibility of KeAi Communications Co., Ltd.
* Corresponding author.
** Corresponding author.
E-mail addresses: xinquanjiang@aliyun.com (X. Jiang), byuxing@ccmu.edu.cn (Y. Bai).

https://doi.org/10.1016/j.bioactmat.2022.01.021
Received 21 July 2021; Received in revised form 23 December 2021; Accepted 17 January 2022
Available online 6 February 2022

movement through stimulating bone remodeling. These researches manifested the pivotal role of bone remodeling in the acceleration of orthodontic tooth movement.

During orthodontic treatment, the primary rate-limiting factor for tooth movement is bone resorption in the interface between the alveolar bone and periodontal ligament (PDL) in the compressive side of the force stimulated teeth. Bone modeling as the un-coupled process of bone resorption and formation causes the changes of the shape, position and size of the bone [8]. Meanwhile, bone remodeling as a tightly coupled process is consists of the reversal phase and bone formation phase after the bone resorption in the same local position, which results in the bone turnover through replacing old bone with new bone [9]. Both of the

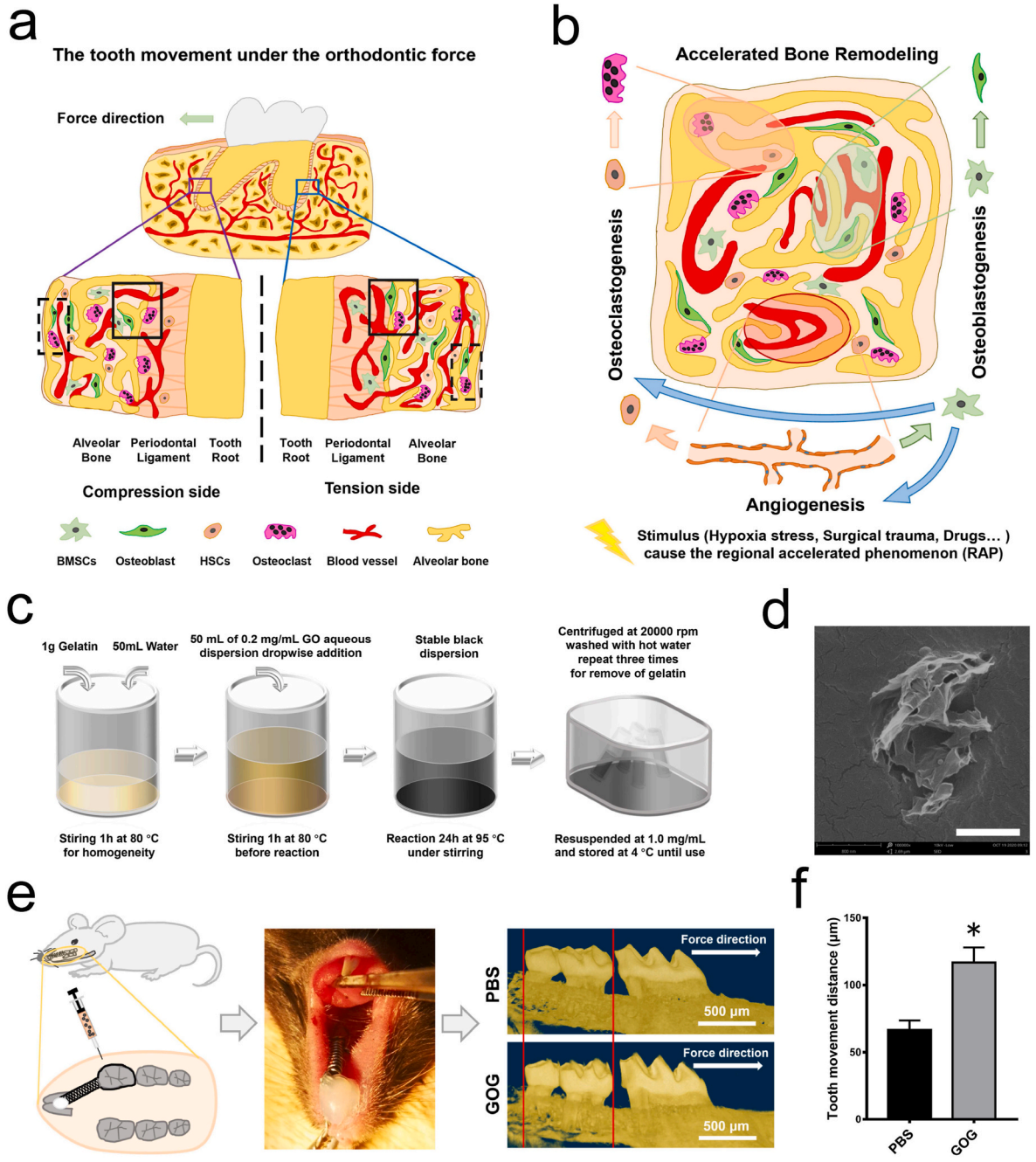

Fig. 1. Schematic diagram of the orthodontic treatment physiological basis and regional acceleratory phenomenon (RAP), GOG local injection promoted the orthodontic tooth movement *in vivo*. **(a)** Under the stress stimulation, the tooth moves in the force direction with bone modeling (indicated in solid box) and remodeling (indicated in dotted box). The compression and tension sides of the tooth root illustrate the different locations of the bone resorption and formation activities. The osteoblast/osteoclast progenitors and vascular tissues compose the physiological basis, which response to the compress/tense force and interact with each other forming the processes of bone modeling and remodeling. **(b)** With the stimulus such as hypoxia, trauma and drugs treatment, the bone remodeling would be accelerated with active osteoblastogenesis, osteoclastogenesis and angiogenesis. The BMSCs as the osteoblast progenitor play a pivotal role in response to the external stimulus and regulate the osteoclastogenesis and angiogenesis. Meanwhile, the angiogenesis also favor the osteoblastogenesis and osteoclastogenesis with providing the well-organized vascular network and recruitment of osteoblast/osteoclast progenitors. **(c)** Schematic diagram illustrated the brief synthetic process of GOG. **(d)** The SEM image of GOG showed the surface morphology, bar: 800 nm. **(e)** Micro-CT analysis showed that the local injection of GOG around the maxillary left first molar could accelerate the tooth movement compared with the control group with PBS injection. **(f)** The quantitative analysis of the tooth movement distance in both GOG and PBS injection groups. *$p < 0.05$ indicates significant difference compared to PBS group.

bone modeling and remodeling are involved with the cellular activities of osteoblastogenesis, osteoclastogenesis and angiogenesis in the activity areas (Fig. 1a), which act as the determinants for the rate of orthodontic tooth movement [10]. The bone resorption as the rate-limiting factor for tooth movement, is determined by the number and function of osteoclasts. The differentiation and maturation of osteoclast progenitors are regulated by the protein factors that were secreted by stromal and osteoblastic cells. Among the biological molecules, the macrophage colony-stimulating factor (M-CSF) functions as the important factor for the recruitments and differentiation of osteoclast progenitors [11]. Meanwhile, the ratio of receptor activator of nuclear factor kappa B ligand (RANKL) to osteoprotegerin (OPG) secreted by stromal and osteoblastic cells and the expression of the receptor activator of nuclear factor kappa B (RANK) in osteoclast progenitors play a crucial determinative roles in the differentiation and function maturation of osteoclast progenitors [12]. The expressions of vascular endothelial growth factor (VEGF) and its receptor VEGFR were detected in the stromal and osteoblastic cells, which could induce the RANKL expression via the autocrine regulatory effect of VEGF [13]. In the corticotomy procedures, the disturbed vascular network caused the local hypoxic microenvironment and the increased expressions of hypoxia inducible factor (HIF) in stromal and osteoblastic cells resulted in the up-regulation of VEGF and RANKL, which further induced the differentiation of osteoclast progenitors into functional osteoclasts [14]. The histological observations also showed the more obvious bone resorption and bone formation around the newly formed vascular plexus due to the increased expression of VEGF in the corticotomy treatment [15]. Meanwhile, the inflammation cytokines, including IL-1β, IL-6 and TNF-α, could promote the differentiation and function maturation of osteoclast, which activated the bone remodeling and accelerated the orthodontic tooth movement [16–18]. These previous researches showed the closely interaction among the osteoblastogenesis, osteoclastogenesis and angiogenesis processes in the bone remodeling during the orthodontic tooth movement.

Under the local hypoxic microenvironment induced by the corticotomy, the reactive oxygen species (ROS) usually accumulates to affect the cellular functions resulting in the altered bone remodeling. The endoplasmic reticulum (ER), as an organelle responsible for protein synthesis and modification, usually plays an important regulatory effects on cellular behavior and fate under different conditions. Various stimuli including oxidative stress, calcium depletion and nutrition deprivation, usually disturb the cellular homeostasis and cause the accumulation of unfolded or misfolded proteins in the ER cavity, which leads to ER stress [19]. The unfolded protein response (UPR) would be induced by ER stress to alleviate the imbalance between the unfold proteins and the capacity of ER on protein synthesis and modification, in which the double-stranded RNA-dependent protein kinase-like ER kinase (PERK) signal pathway plays a pivotal regulative effect on the cellular response to ER stress during UPR [20]. Eukaryotic initiation factor 2α (eIF2α), as the downstream protein factor of PERK pathway, its phosphorylation by activated PERK would further influence the mRNA translation and protein synthesis under the stimuli [21]. Through the UPR regulation on the cellular behavior, the differentiation and function of the related progenitor cells with ER stress would adapt to another appropriate states for attainment of the new homeostasis, which would result in an more active bone remodeling during the corticotomy. These indicate that the ER stress caused by stimuli, like hypoxia and reactive oxygen species in corticotomy, maybe has an important regulatory effects on the cellular behavior in the bone remodeling, which would induce the regional acceleratory phenomenon (RAP) and accelerate the orthodontic tooth movement.

The pluripotent stem cells that reside in the alveolar bone marrow, periodontal ligament and periosteum, usually function as the regulatory cells in bone remodeling and influence the rate of orthodontic tooth movement. Bone marrow stromal stem cells (BMSCs) has been reported to express multiple intra- and extra-cellular molecules, including VEGF, surviving p21, caspases and others, and these signaling molecules have the pro-survival and pro-angiogenic effects on the BMSCs themselves and other cells under the hypoxic conditions [22,23]. Meanwhile, the inflammatory cytokines, including TGF-β, IL-1β and TNF-α, could stimulate BMSCs to secret VEGF [24], which would directly reverse-act on BMSCs to express the chemotactic factors neurohilin1/2 for the recruitment of osteoprogenitor cells [25]. Besides, as the osteoblast progenitors, BMSCs also secret the related protein molecules to regulate the differentiation of osteoclast progenitors. Overall, under the mechanical, hypoxic and inflammatory conditions during orthodontic treatment or corticotomy surgery, the BMSCs could response to the stimuli so as to regulate their own cell fate and also affect the recruitment of other progenitors for osteoblastogenesis, osteoclastogenesis and angiogenesis, which would determine the activity level of bone remodeling and the rate of tooth movement (Fig. 1b). The hematopoietic stem cells (HSCs) that reside alongside the bone marrow cavity, as the primary osteoclast progenitors, could give rise to the bone marrow derived macrophage (BMMs) and further differentiate into the mature and functional osteoclast [26]. The differentiation of BMMs in different microenvironment involves the M1/M2 polarization and the imbalance of the polarization would influence its osteoclastic differentiation. The previous researches reported that the M2 polarization of BMMs would enhance the mature osteoclast differentiation [27], and the elevated ER stress could promote the M2 polarization of macrophage [28]. Meanwhile, calcium oscillation induced by RANKL was also reported as a key factor to osteoclast differentiation [29] and the ER stress usually involved the calcium transfer due to the role of ER as intracellular calcium pool [30]. Besides, the calcium signaling also control the growth and differentiation of BMSCs, and related downstream signaling pathways can be activated through the release of Ca^{2+} from endoplasmic reticulum to elicit its regulatory effects on BMSCs differentiation [31]. During the ER stress, the efflux of Ca^{2+} from endoplasmic reticulum would function as an important regulative signaling on the cellular behaviors, and the UPR induced by ER stress also could promote the RANKL expression in primary osteoblastic progenitors [32]. All the previous reports suggest some potential correlations among the ER stress, osteoblastogenesis and osteoclastogenesis. In a view of all the cellular activities during the bone remodeling, we hypothesize that BMSCs as the most critical candidate for active functional cell has an important regulatory effects on the osteoblastogenesis, osteoclastogenesis and angiogenesis during bone remodeling activation.

Graphene based materials as novel nanosheet biomaterials has potential applications in many biomedical fields [33], and the hypoxia stimulation induced by reduced graphene oxide could promote the angiogenic differentiation of mesenchymal stem cells [34] and accelerate the bone tissue regeneration repair [35]. In our previous study, we have prepared and characterized the gelatin reduced graphene oxide (GOG). The study on its biological properties showed that GOG had a good biocompatibility and could synergistically promote osteogenesis of bone marrow stromal stem cells (BMSCs) with delivery of pro-osteogenic drugs [36]. Besides, the hydrogel composite reinforced with GOG could promote bidirectional osteogenic/angiogenic differentiation of BMSCs through the reactive oxygen species (ROS) stimulation due to the hypoxic microenvironment caused by GOG [37]. All these previous studies on GOG suggest that graphene materials could induce the local hypoxic microenvironment with appropriate dose application, which indicates its potential application in triggering the regional acceleratory phenomenon (RAP) with the positive regulatory effect on bone remodeling and orthodontic tooth movement. Hence, whether the local application of GOG could accelerate the orthodontic tooth movement and whether the BMSCs indeed play an pivotal regulatory effects on promotion of the osteoblastogenesis, osteoclastogenesis and angiogenesis during the GOG stimulation are the scientific questions worthy of detailed explorations. Meanwhile, the potential relevant mechanism underlying this graphene application strategy for accelerating orthodontic tooth movement is also needed to be clarified in details so as to

provide a reference for further application of the novel biomaterials in orthodontic treatment.

In this study, we evaluated the effects of GOG on bone remodeling and verify the promotive effect of GOG on the acceleration of tooth movement *in vivo*. Meanwhile, the *in vitro* observation on the sub-cellular location of GOG in BMSCs showed its adjacent distribution with ER, and this spatial location proximity indicated that the PERK signal pathway may play a potential role in the regulatory effects of the GOG stimulated BMSCs on the osteoblastogenesis, osteoclastogenesis and angiogenesis in the UPR. The aggregation of GOG in the spleen and the activation of monocyte/macrophages in the marginal zone and red pulp showed the regulatory effect of GOG on the genesis of the osteoclast progenitors *in vivo*. Subsequently, we further investigated the biological effects of the GOG stimulated BMSCs on the osteoclastogenesis of HSCs and the angiogenesis of HUVECs *in vitro*. We also evaluated the detailed osteoclastogenesis of HSCs in the aspects of the BMMs differentiation and its further M1/M2 polarization. The angiogenesis of HUVECs was analyzed to clarify the pro-angiogenic effect of the GOG stimulated BMSCs. The mechanism analysis on the biofunctions of the GOG stimulated BMSCs illustrated the important regulatory effects of PERK pathway on the osteoblastogenesis, osteoclastogenesis and angiogenesis, in which the endoplasmic reticulum (ER) stress caused by GOG in BMSCs induced the unfold protein response (UPR) and activated PERK pathway to elicit its further regulatory effects on bone remodeling. Combining the results of the orthodontic tooth movement model *in vivo* and the co-culture of GOG stimulated BMSCs with HSCs or HUVECs *in vitro*, we first proposed the promised application of GOG in the acceleration of orthodontic tooth movement. This research would provide a novel biomaterials choice for inducing the RAP with promoting bone remodeling, and these results also expanded the application field of GOG in the field of oral medicine.

2. Materials and methods

2.1. Preparation of gelatin reduced graphene oxide

The graphene oxide was reduced by the gelatin to obtain the gelatin reduced graphene oxide (GOG) as our previous description [37]. The characterization of GOG was conducted by scanning electron microscope (SEM) to detect the surface morphology of GOG.

2.2. Local injection of GOG in the mouse orthodontic tooth movement (OTM) model

The 8-weeks-old C57BL/6 mice were anaesthetized with 1% chloral hydrate intraperitoneal injection (0.4 mL/10 g weight). Nickel titanium tension springs (Tomy, Japan) were used to offer 20 g force to the maxillary left first molar by stainless steel ligation wire fixation, and the front end was fixed on the maxillary incisor using a resin ball. After establishing the OTM model, the 20 μL 10 mg/mL GOG solution was immediately applied through buccal submucous local injection around the maxillary left first molar as the experimental group, and phosphate buffer saline (PBS) solution injection served as the control group. The intraperitoneal injection 35 mg/kg Alizarin Red S (AL) at 0 day and 30 mg/kg Calcein (CA) at 7 day was carried out for the sequential fluorescent labeling of the bone formation. Every group contained 6 mice, all the animal experiments were approved by the Animal Ethics and Welfare Committee of Beijing Stomatological Hospital. For further verification on the effect of PERK pathway in promoting bone remodeling *in vivo*, the co-injection of GOG with GSK2606414 (0.1 μM, a small molecule compound can bind to the PERK kinase domain and inhibit PERK activation) was conducted to observe the changes of tooth movement due to the block of PERK pathway.

2.3. Observation and histological analysis on the tooth movement

The mice were sacrificed for sample harvest through cervical dislocation after 10 days powder soft diet. The distance between the first molar and posterior teeth was recorded with stereomicroscope image. Micro-CT scan of the samples were also conducted to detect the bone remodeling around the teeth. The 5 μm paraffin sections were performed after decalcification with 10% EDTA, and the Hematoxylin-eosin (HE) and Tartrated resistant acid phosphatase (TRAP) stainings were conducted to observe the histological differences between the different groups during tooth movement. The hard tissue sections were prepared for observation on the new bone formation labeled by sequential fluorochrome, as previously described [37]. For observation on the distribution of the osteoblastic marker (Runx2) and the PERK downstream effector protein (p-eIF2α) *in vivo*, the immunofluorescent staining was conducted so as to clarify the relationship between the osteoblastic differentiation and the PERK pathway. The sections were firstly deparaffinated and treated with citric acid buffer (pH 6.0) microwave antigen retrieval for the subsequent antigen blocking and primary antibody incubation. The Cy3-conjugated and FITC-conjugated secondary antibodies were used to detect the Runx2 and p-eIF2α respectively, and the nucleus was stained with DAPI for further observation under the fluorescent microscope. The HE staining was conducted after the immunofluorescent staining of Runx2 and p-eIF2α to observe the histological differences among the groups.

2.4. Isolation and culture of bone marrow mesenchymal stem cells (BMSCs) and hematopoietic stem cells (HSCs)

The 6-weeks-old C57BL/6 mice were used to collect the bone marrow content of the femurs and tibias flushed by the Minimum Essential Medium α (α-MEM) culture media supplemented with 10% Fetal Bovine Serum and 1% Penicillin/Streptomycin. The bone marrow cells mixture were cultured in an incubator at 37 °C with 5% CO_2. After 72 h, the attached BMSCs were obtained and the fresh complete medium was replaced every other day for further expansion and passage of BMSCs. Meanwhile, after 24 h, the supernatant of the cultured bone marrow cells mixture were extracted and collected for isolation of the non-adherent HSCs according to the methods described by Maridas et al. [26]. The HSCs were used as the progenitor cells to obtain the adherent bone marrow-derived macrophages (BMMs) with M-CSF (50 ng/mL) induction, and the osteoclast differentiation media containing 50 ng/mL M-CSF and 100 ng/mL RANKL were used to induce osteoclastic differentiation of BMMs for further experimental analysis.

2.5. Sub-cellular location of GOG in BMSCs and the distribution of GOG in organs

The medium containing 1 mg/mL GOG was used to culture BMSCs for further analysis on the location of GOG in cells. The transmission electron microscope (TEM) was performed to observe the location of GOG in BMSCs as our previous description [38]. For detailed detection on the spatial location relationship between GOG and endoplasmic reticulum or mitochondria, the GOG was labeled with Rhodamine-6G (R6G) to get R6G labeled GOG as previous description [36] and the GOG endocytosed BMSCs were stained with ER-tracker Green (C1042S, Beyotime, China) or Mito-tracker Green (C1048, Beyotime, China) for visualization of endoplasmic reticulum or mitochondria under the fluorescent microscope respectively. JC-1 (40705ES03, Yeasen, China) was used to analysis the change of the mitochondrial membrane potential due to GOG stimulus as the protocol description. When the mitochondrial membrane potential increases, the monomers of JC-1 would form the polymers of JC-1 resulting in the change of fluorescence properties. The monomers and polymers of JC-1 can be detected with the emission wavelengths of 525 nm (green) and 590 nm (red) at the excitation wavelengths of 490 nm and 530 nm respectively. The ROS

detection were conducted using the ROS Assay Kit (50101ES01, Yeasen, China) as previous description [38]. The calcium concentration in the BMSCs was detected using the calcium binding dye Fluo-4 AM (S1060, Beyotime, China) according to the protocol of the manufacturer.

After the buccal submucous injection of R6G labeled GOG, the mice were sacrificed 24 h after the OTM surgery for analysis on the distribution of R6G labeled GOG in the organs. The different organ samples were embedded in paraffin and cut into sections for observation under the fluorescent microscope. Due to the aggregation of GOG was detected in spleen, the further observation on the spleen was conducted in details so as to analyze the effects of GOG on spleen biofunction. The spleen samples collected 24 h after GOG local injection surgery were embedded with tissue OCT-freeze medium for frozen sections, and the sections were fixed with 4% paraformaldehyde (PFA) solution for subsequent immunofluorescent staining on macrophage marker CD11b. The FITC-conjugated secondary antibody was used to detected the expression of CD11b (ab8878, Abcam, USA), then cytoskeleton was stained with Actin-Tracker Red-555 (C2203S, Beyotime, China) and nucleus was stained with DAPI for the final observation under the fluorescent microscope. After the fluorescent observation, the sections were counterstained with HE for the histological images using optical microscope.

2.6. Evaluation about the biological effects of GOG stimulated BMSCs on osteoclastogenesis and angiogenesis

The transwell co-culture of BMSCs with HSCs was used to analyze the pro-osteoclastogenesis effect of GOG stimulated BMSCs. The transwell inserts with 0.4 μm pore size of the translucent membranes were used in our experiments, which just allowed the communications of the proteins and ionic molecules without the permission of cellular migration and penetration. The upper chamber was seeded with BMSCs cultured with the GOG medium (the concentration of GOG was 1 mg/mL), and the HSCs were cultured in the lower chamber with M-CSF (50 ng/mL) for inducing BMMs differentiation of HSCs. After 4 days M-CSF induction, the Flow cytometry analysis was conducted to evaluate the proportion of BMMs in total HSCs. The osteoclast differentiation media containing 50 ng/mL M-CSF and 100 ng/mL RANKL was replaced at day 5 in the lower chamber for further analysis on osteoclastic differentiation of BMMs. In the subsequent induction of BMMs, the M1/M2 polarization was detected by M1/M2 specific markers (iNOS and arginase) immunofluorescent staining after 2 days of M-CSF + RANKL induction, and mature osteoclast differentiation was verified by TRAP staining after 6 days of M-CSF + RANKL induction. The calcium oscillation of BMMs was also detected after 2 days of M-CSF + RANKL induction. The procedure about flow cytometry assay, immunofluorescence assay and calcium oscillation measurement were described in details at the subsequent sections. The ALP staining of the BMSCs after 4 days co-culture with HSCs and M-CSF induction was conducted as our previous description [36]. After 10 days of co-culture (4 days of M-CSF induction and 6 days of M-CSF/RANKL combination induction), the ARS staining of the BMSCs was also performed as our previous description [36].

The transwell co-culture of BMSCs with HUVECs was used to analyze the pro-angiogenesis effect of GOG stimulated BMSCs. The upper chamber was seeded with BMSCs cultured with GOG medium, and the HUVECs were cultured in the lower chamber for further evaluation on its migration, sprouting and permeability abilities. The wound healing test was conducted directly with the HUVECs cultured in the lower chamber. For further analysis on the sprouting and vascular permeability of HUVECs, the HUVECs cultured in the lower chamber was detached by trypsin after 3 days co-culture with GOG stimulated BMSCs, and the pretreated HUVECs was seeded in the μ-Slide Angiogenesis ibiTreat microplate for sprouting assay and seeded into the transwell upper chamber with subsequent addition of the FITC-dextran (70 kDa, 46945, Sigma-Aldrich, USA) for permeability evaluation. The fluorescent intensity of the lower chamber medium was measured using the fluorescence microplate reader to detect the permeability of the HUVECs that has been co-cultured with GOG stimulated BMSCs for 3 days. The details about the migration and sprouting assays were described in the below sections.

For further verification on the effect of PERK pathway in promoting bone remodeling *in vitro*, the co-addition of GOG with GSK2606414 (0.1 μM) was conducted to observe the changes of the osteoblastogenesis, osteoclastogenesis and angiogenesis due to the block of PERK pathway in BMSCs. The PERK pathway was analyzed by Western blot to detect the change of the relevant proteins, including PERK, p-PERK, eIF2α, p-eIF2α. Meanwhile, the relevant osteogenic proteins Runx2, OCN, osteoclastogenic proteins RANKL, OPG and pro-angiogenic protein VEGF were also detected to evaluate the biological effects of the GOG stimulated BMSCs.

2.7. Flow cytometry analysis on the osteoclastogenesis of HSCs and immunofluorescence assay on the M1/M2 polarization of BMMs

After 4 days co-culture with BMSCs and M-CSF induction, the total HSCs were collected from the supernatant and attached cells in the lower chamber. The mixture cells were suspended with antibody diluent and incubated with anti-CD11b and anti-F4/80 antibodies for 30 min. After twice washes with PBS, the samples were analyze using FACS Calibur system to detect the ratio of $CD11b^{+}$, $F4/80^{+}$ BMMs in the total HSCs. For further analysis on the polarization of BMMs after 2 days of M-CSF + RANKL induction, the attached cells in the lower chamber were fixed with 4% paraformaldehyde (PFA) solution for the subsequent M1 specific marker (inducible nitric oxide synthase, iNOS) and M2 specific marker (arginase, ARG) immunofluorescent staining. PE-conjugated anti-mouse CD11b (M1/70, 12-0112-82, Invitrogen, USA) and FITC-conjugated anti-mouse F4/80 (BM8, 11-4801-82, Invitrogen, USA) antibodies were used for the FACS analysis. Anti-iNOS (ab178945, Abcam, USA) and anti-ARG (ab96183, Abcam, USA) antibodies were used to detect the M1/M2 polarization of BMMs.

2.8. Measurement of intracellular calcium oscillation

The calcium oscillations were tested by the calcium binding dye Fluo-4 AM (S1060, Beyotime, China) according to the protocol of the manufacturer. After 2 days induction with osteoclast differentiation media containing 50 ng/mL M-CSF and 100 ng/mL RANKL, the BMMs in the lower chamber were washed with PBS buffers and incubated with 2 μM Fluo-4 AM staining solution for 30 min at 37 °C. After the Fluo-4 AM probe loading, the BMMs were washed with PBS once again and incubated with osteoclast differentiation media for another 30 min. The 520 nm fluorescent intensity of the BMMs were detected with the fluorescence microplate reader using excitation wavelength of 488 nm, and the sequential detection were performed with 2 s interval for 5 min for analysis on calcium flux.

2.9. Migration and sprouting assays on angiogenesis of HUVECs

HUVECs were seeded in the low chamber with the subsequent scratch fabrication using the pipette tip and BMSCs were seeded in the upper chamber with GOG stimulation, the gaps of the HUVECs were observed with microscope imaging after 24 h to evaluate the migration ability of HUVECs. For analysis on the angiogenesis of HUVECs, after 3 days co-culture with the GOG stimulated BMSCs, the HUVECs were detached using trypsin for sprouting assays. The thawed Matrigel was added into the lower well of the μ-Slide Angiogenesis ibiTreat microplate with 10 μL per well on ice, and the microplate was transferred into cell culture incubator for 30 min to allow the Matrigel to solidify. The detached HUVECs were seeded on the Matrigel with the 4×10^3 per well and cultured for 4 h. The microplate was observed under optical microscope to capture the sprouting images. The number of the circle and nude points per field were analyzed using the NIH ImageJ 1.45 software as our previous description [37]. All assays were repeated three times.

2.10. Aortic ring assay

The thoracic aortas were excised from 8-weeks-old SD rats and were cut into cross-section rings with 1 mm length as described by Zeng et al. [39]. The aortic rings were cultured with the DMEM medium with 10% Fetal Bovine Serum and 1% Penicillin/Streptomycin supplemented with 10 ng/mL vascular endothelial growth factor (VEGF). After 24 h incubation, aortic rings were fixed in the Matrigel-coated low chamber with incubation at 37 °C for 30 min to allow the Matrigel to solidify. Subsequently, the upper chamber of the transwell was seeded with BMSCs, GOG stimulated BMSCs and GOG + GSK2606414 stimulated BMSCs for analysis on the pro-angiogenic effects of different groups. After 5 days co-culture with the GOG stimulated BMSCs, the number of new sprouts from the aortic rings was observed with microscope image. All assays were repeated three times.

2.11. Quantitative RT-PCR analysis

The total RNA of the BMSCs after 4 days co-culture with HSCs, BMMs after 6 days of M-CSF + RANKL induction and HUVECs after 3 days co-culture with BMSCs were collected as the previous description [37]. The cDNA was synthesized using the NovoScript® Plus All-in-one 1st Strand cDNA Synthesis SuperMix (Novoprotein Scientific, China) and the real-time PCR was conducted using the NovoStart® SYBR qPCR SuperMix Plus (Novoprotein Scientific, China). The relevant osteogenic, osteoclastogenic and angiogenic genes were detected with $2^{-\Delta\Delta Ct}$ methods. The primer sequences were listed in Table 1.

2.12. Western blot analysis

After 12 h co-culture with HSCs and M-CSF stimulation, the total proteins of the BMSCs under the control medium, GOG medium and GOG + GSK2606414 medium were collected using RIPA lysate with addition of phosphatase inhibitor cocktail. The protein expressions of PERK, p-PERK, eIF2α, p-eIF2α and Runx2 in BMSCs were tested after 12 h co-culture with HSCs and M-CSF stimulation. The total protein of BMSCs were also collected after 2 days of M-CSF + RANKL induction and the expressions of OCN, RANKL, OPG and VEGF were measured to evaluate the change of BMSCs due to the GOG stimulation with BMMs co-culture and M-CSF + RANKL induction. The primary antibodies against PERK (#3192, CST, USA), p-PERK (#3179, CST, USA), eIF2α (#5324, CST, USA), p-eIF2α (#3398, CST, USA), Runx2 (ab23981, Abcam, USA), OCN (ab93876, Abcam, USA), RANKL (ab9957, Abcam, USA), OPG (ab183910, Abcam, USA), VEGF (ab1316, Abcam, USA) and β-actin (ab8227; Abcam, USA) were used in this research. The quantitative evaluation on the protein expression level was conducted using the NIH ImageJ 1.45 software with the β-actin as the internal control.

Table 1
The primer sequences of the genes detected in this study.

Gene	Forward and reverse sequences (5′ to 3′)
mGAPDH-F	TGAGGCCGGTGCTGAGTATGTCG
mGAPDH-R	CCACAGTCTTCTGGGTGGCAGTG
mALP-F	TGCCTACTTGTGTGGCGTGAA
mALP-R	TCACCCGAGTGGTAGTCACAATG
mRunx2-F	CACTGGCGGTGCAACAAGA
mRunx2-R	TTTCATAACAGCGGAGGCATTTC
mCol1-F	ATGCCGCGACCTCAAGATG
mCol1-R	TGAGGCACAGACGGCTGAGTA
mOcn-F	AGCAGCTTGGCCCAGACCTA
mOcn-R	TAGCGCCGGAGTCTGTTCACTAC
mRANKL-F	ACCAGCATCAAAATCCCAAG
mRANKL-R	TTTGAAAGCCCCAAAGTACG
mOPG-F	GTTCTTGCACAGCTTCACCA
mOPG-R	AAACAGCCCAGTGACCATTC
mVEGF-F	ACGCATTCCCGGGCAGGTGAC
mVEGF-G	TCTTCCGGGCTTGGCGATTTAG
mTRAP-F	TGGTCATTTCTTTGGGGCTTATCT
mTRAP-R	GCTACTTGCGGTTTCACTATGGA
mCTSK-F	TGACCACTGCCTTCCAATAC
mCTSK-R	CTCTGTACCCTCTGCATTTAG
mRANK-F	GTCTGCAGCTCTTCCCTGAC
mRANK-R	GAGGAGCAGGACGATGAGAC
mMMP9-F	CGTGTCTGGAGATTCGACTTGA
mMMP9-R	TTGGAAACTCACACGCCAGA
β-actin-F	CCTTCCTGGGCATGGAGTCCTG
β-actin-R	GGAGCAATGATCTTGATCTTC
vWF-F	CCCCTGAAGCCCCTCCTCCTA
vWF-R	ACGAACGCCACATCCAGAACC
CD31-F	CAACGAGAAAATGTCAGA
CD31-R	GGAGCCTTCCGTTCTAGAGT

2.13. Statistical analysis

The statistical comparisons were performed using one-way ANOVA and Student–Newman–Keul (SNK) tests after the normal distribution and equal variance assumption test. The quantitative data were expressed as means ± SD, and the statistical analysis was performed with SAS 8.2 statistical software package (Cary, USA). The differences were considered statistically significant at the confidence levels above 95% (*$p < 0.05$).

3. Results and discussions

3.1. The acceleration of tooth movement induced by GOG local injection in vivo

The synthetic process of the gelatin reduced graphene oxide (GOG) was briefly indicated as the schematic diagram (Fig. 1c). The SEM image of GOG showed its surface topography (Fig. 1d) and the detailed characterization of GOG had been reported in our previous research [36]. After local injection of GOG solution around the maxillary left first molar that was ligated with tension springs in the mouse orthodontic tooth movement model, the micro-CT analysis on the tooth movement showed that the injection of GOG can accelerate the speed of the tooth movement (Fig. 1e). The distance between the maxillary first molar and its posterior teeth was increased in the GOG local injection group compared with the PBS control group (Fig. 1f) after 10 days of orthodontic treatment.

The section images of the micro-CT (Fig. 2a) showed the wider low density periodontal membrane image (white arrow indicates the positions) in the root mesial side of the GOG injection group. The unresorption of the alveolar bone were detected in the PBS injection group (yellow arrow indicates the positions), which limited the tooth movement under the stress stimulus. The periodontal membrane image of the root distal side (white triangle indicates the positions) also showed a difference in the bone density, the low density new bone image can be detected in the GOG injection group which showed a rapid osteogenesis. The line profile of the gray values (Fig. 2b) also showed that the GOG injection group had a more wider mesial periodontal membrane image (red dotted line indicates the positions) and narrower distal periodontal membrane image (green dotted line indicates the positions) compared with the PBS injection group. Through the above radiographic observation on the rapid bone resorption and tooth movement acceleration in GOG group, we could speculate that the bone remodeling was accelerated due to the GOG local injection. The histological sections showed the detailed changes around the root. The TRAP staining (Fig. 2c) presented the more osteoclasts around the compression side of first molar roots and the more new bone formations were also observed around the interradicular septa between the mesial and distal buccal roots of first molar at the sequential fluorescence labeling images (Fig. 2d), which showed the more active bone remodeling in the GOG injection group compared with PBS group. The quantitative analysis of the fluorochrome stained bone (Fig. 2e) showed that the more new bone formation activities were labeled by AL and CA. The magnified field of TRAP staining (Fig. 2f) showed that the more osteoclasts were detected

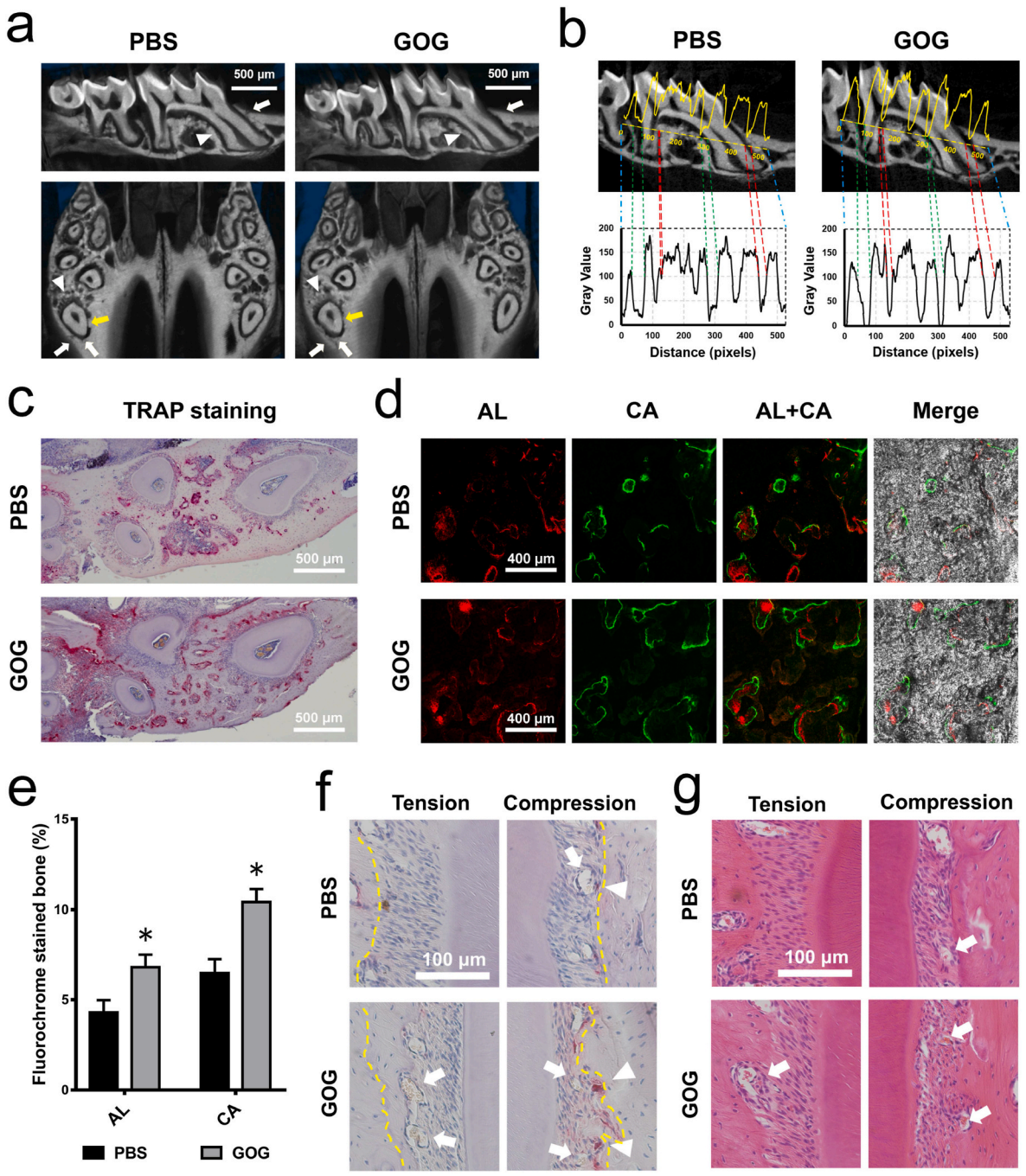

Fig. 2. The micro-CT and histological examination on the orthodontic tooth movement *in vivo* showed the more active bone remodeling in GOG injection group. **(a)** The sagittal and transversal sections of the micro-CT showed the changes of the alveolar bone around the tooth. White arrow indicates the mesial periodontal membrane image which represents the activity of bone resorption and yellow arrow shows the delayed bone resorption in PBS group, white triangle indicates the distal periodontal membrane image which represents the activity of bone formation, bar: 500 μm. **(b)** The line profile of the gray values in the sagittal sections. The red and green dotted line indicates the mesial and distal periodontal membrane width of the root respectively. **(c)** The TRAP staining of the sections showed the more detected osteoclast activities (the purple stained position indicates the mature osteoclast) in GOG group compared with PBS group, bar: 500 μm. **(d)** The sequential fluorescence labeling images showed the activity level of the new bone formation, which was labeled through the intraperitoneal injection Alizarin Red S (AL) at 0 day and Calcein (CA) at 7 day after the establishment of OTM model, bar: 400 μm. **(e)** The quantitative analysis of the fluorochrome stained bone showed the increased bone formation in GOG group compared with PBS injection groups. *$p < 0.05$ indicates significant difference compared to PBS group. **(f)** The magnified field of the TRAP staining showed the detailed bone formation and resorption activities. The white arrow indicates the blood vessels and triangle indicates the mature osteoclast, yellow dotted line indicates the border between the new bone formation/bone resorption and the old bone structure, bar: 100 μm. **(g)** The HE staining also showed the similar condition of bone remodeling (bone formation, bone resorption and angiogenesis). The white arrow indicates the blood vessels, bar: 100 μm.

in the compression side of the GOG group (triangle indicates the osteoclasts, yellow dotted line showed the bone resorption border) and the new bone formation was also more obvious in the tension side of the GOG group (yellow dotted line showed the border between the new bone formation and old bone structure). Meanwhile, the more blood vessels were detected around the bone resorption and bone formation sites (white arrow indicates the positions), which indicated the pivotal role of vascular network in active bone remodeling. Consistent with the

TRAP results, the HE staining (Fig. 2g) illustrated the similar bone resorption and formation status around the root, which also showed the more blood vessels (white arrow indicates the positions) in the GOG group compared with the PBS control group. Meanwhile, the osteoclast induced bone resorption and osteoblast induced bone formation were also more detected around the blood vessels in the GOG injection group. All the results indicated that the bone remodeling in the GOG treated group was accelerated with promoted osteoblasto-/osteoclasto-genesis and angiogenesis.

3.2. The sub-cellular location of GOG in BMSCs and the aggregation of GOG in spleen

The TEM observation of the distribution of GOG in the BMSCs after culturing by GOG medium with different times (Fig. 3a) showed that the GOG was located around the endoplasmic reticulum and mitochondria (white arrow indicates the location of GOG), and the degradation of the GOG was observed as the small short residue chains (white triangle indicates the degraded fragments). The degradation fragments of GOG observed in our report was similar to the morphological character of the Nitric Oxide (NO)-dependent biodegradation of graphene oxide (GO) described by Peng et al. [40], which indicated the good biodegradation of GOG in BMSCs. The ER-tracker Green staining results (Fig. 3b) showed that the GOG was located around the endoplasmic reticulum, which indicated its influence on ER stress and induction of the unfolded protein response (UPR). The Mito-tracker Green staining (Fig. 3b) also showed the adjacent distribution of GOG with mitochondria, the near location relationship would arise the integrated stress response to regulate the cell functional status [41]. The differentiation of BMSCs need a high energy consumption, and the activity of the mitochondria

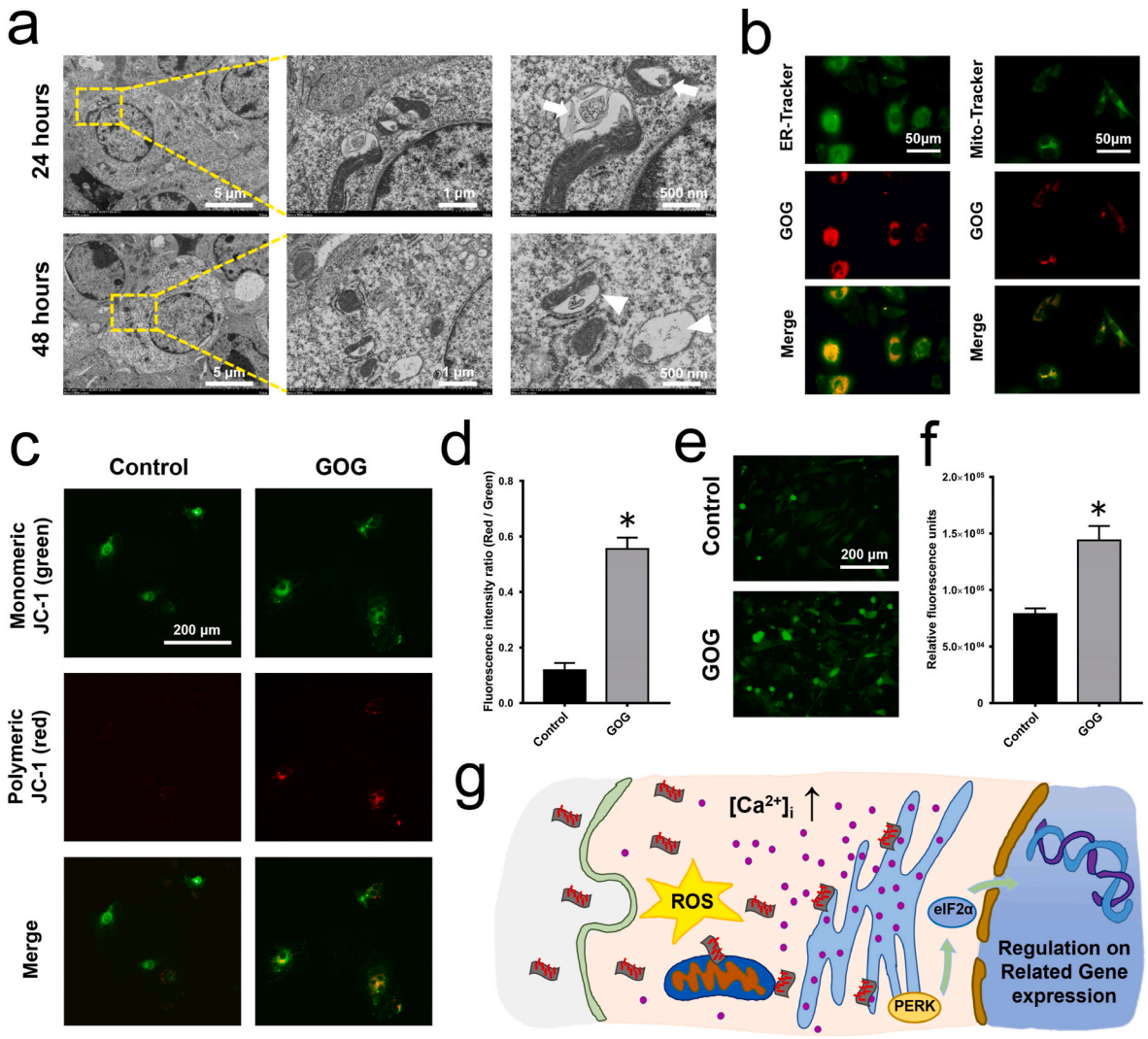

Fig. 3. The sub-cellular location of GOG in BMSCs and its probable regulatory mechanism *in vitro*. **(a)** The TEM images showed the distribution of GOG in BMSCs after different treatment times, the white arrow indicates the near location of GOG with endoplasmic reticulum and mitochondria, white triangle indicates the degraded fragments of GOG. **(b)** The ER-tracker Green and Mito-tracker Green staining showed the co-location of the R6G labeled GOG with the endoplasmic reticulum and mitochondria, bar: 50 μm. **(c)** The BMSCs cultured with control medium and GOG medium were stained by JC-1, the polymeric JC-1 was detected as red signal due to the high mitochondrial membrane potential and the monomeric JC-1 was detected as green signal in the ordinary mitochondrial membrane potential, bar: 200 μm. **(d)** The quantitative analysis of the red/green fluorescence intensity showed the ratio of polymeric to monomeric JC-1 under different culture media. *p < 0.05 indicates significant difference compared to the control group. **(e)** The ROS level detected by DCFH-DA fluorescent probe was observed under the fluorescent microscope, the fluorescent intensity represent the intracellular ROS level, bar: 200 μm. **(f)** The quantitative analysis of the calcium ion fluorescent intensity detected using the Fluo-4 AM probe showed the increased calcium concentration in GOG stimulated BMSCs compared with the normal control group. *p < 0.05 indicates significant difference compared to the control group. **(g)** The schematic diagram presents the sub-cellular location of GOG in BMSCs and its probable mechanism on regulating cellular behaviors.

plays an important supportive role in the BMSCs osteogenesis. The JC-1 dye was used to stain the BMSCs under different culture medium (Fig. 3c), the GOG medium treated BMSCs showed an increase of the polymeric JC-1 (which was detected as red signal due to high mitochondrial membrane potential), which indicated that the mitochondrial membrane potential increased with the stimulation of GOG and the BMSCs had a high mitochondrial activity so as to maintain its endocytosis the degradation of GOG for its further differentiation and regulation activities. The ratio of polymeric to monomeric JC-1 (which was detected as green signal under the normal mitochondrial membrane potential) (Fig. 3d) also showed the increased mitochondrial activity due to GOG stimulus.

The intracellular ROS level detection (Fig. 3e) showed an increased fluorescent intensity in the GOG stimulated BMSCs, which indicated that the mitochondrial stress induced by GOG proximity effect would cause the integrated stress response for further regulation on cellular behaviors. Meanwhile, the quantitative analysis on the fluorescent intensity of the calcium ion concentration in BMSCs showed an about 80% increase in GOG stimulated BMSCs compared with the BMSCs cultured with normal medium (Fig. 3f). The increased calcium ion detected in cytoplasm maybe derive from the calcium external-flow from the calcium pool (endoplasmic reticulum) due to the ER stress, which would has an regulatory effects on the growth and differentiation through influencing the expression level of transcription related genes [42,43]. During the UPR caused by ER stress and the integrated stress response caused by mitochondrial stress, the phosphorylation of eukaryotic translation

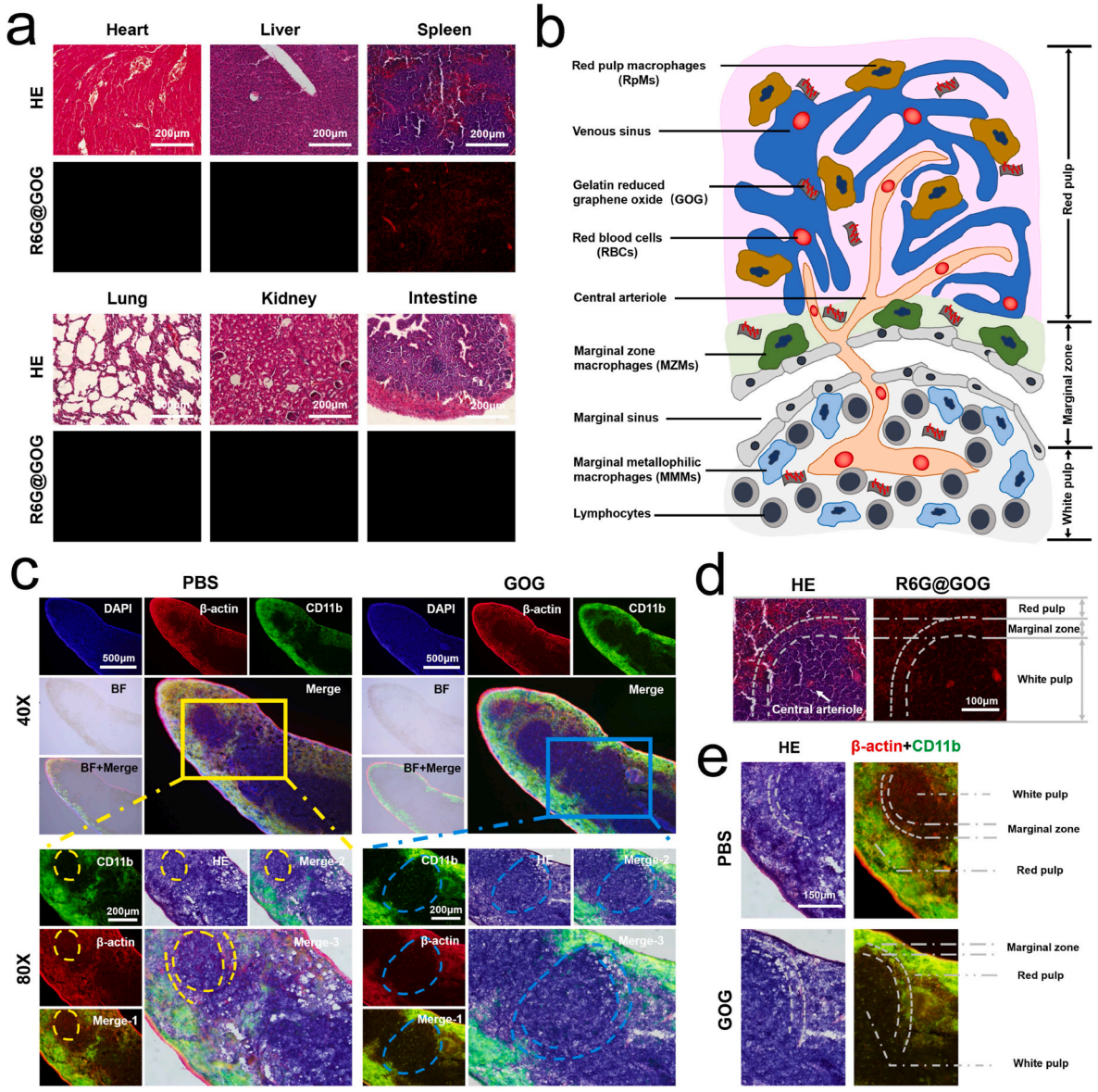

Fig. 4. The distribution of GOG in spleen and its effect on the monocyte/macrophages activation after local injection *in vivo*. **(a)** The sections of different organs showed the aggregation of GOG in spleen, bar: 200 μm. **(b)** The scheme showed the spleen structure and the distribution of GOG in the spleen, and the different monocyte/macrophages located in different sites of the spleen. **(c)** The enlarged white pulp with low density of β-actin staining was observed in the GOG injection group, and the CD11b immunofluorescent staining showed the more active monocyte/macrophages detected in the marginal zone and red pulp of the spleen in the GOG injection group (40 X, bar: 500 μm). In the magnified images, the yellow dot circle showed the white pulp and the yellow dot line showed the border of the marginal zone in the PBS control group; the blue dot circle showed the marginal zone border and the blue dot line showed the white pulp range (80×, bar: 200 μm). **(d)** The magnified image of the GOG aggregation in spleen, bar: 100 μm. **(e)** The magnified details showed the enlarged white pulp of spleen in the GOG injection group, and the CD11b immunofluorescent staining showed the more active macrophages detected in the white pulp and marginal zone of the spleen in the GOG injection group, meanwhile, the CD11b was also high-expressed in red pulp of the GOG group, bar: 150 μm.

initiation factor 2α (eIF2α) can be activated by PERK so as to alleviate the diverse cellular stresses, and the subsequent regulation on the relevant effector proteins would affect the cellular behaviors under the stress stimulus [20,41]. The schematic diagram (Fig. 3g) sketched the possible mechanism of GOG stimulation on the cellular functions of BMSCs. So, in the subsequent experiments we would use the PERK inhibitor GSK2606414 to further clarify the specific regulatory mechanism of GOG on the cellular behaviors.

The sections of the different organs (Fig. 4a) showed that the R6G labeled GOG (R6G@GOG) was mainly detected in the spleen after 1 day of local injection around the maxillary left first molar. The scheme (Fig. 4b) showed the distributions of GOG and macrophages in the spleen. The further analysis on the spleen structure change (Fig. 4c) after GOG injection showed that the white pulp (β-actin staining of white pulp showed a relative low density compared with red pulp) was enlarged, and the more activated monocyte/macrophages (CD11b immunofluorescence staining was positive) was detected in the marginal zone and red pulp of the spleen compared to the PBS control group. The magnified images (Fig. 4d) showed the detailed location of R6G@GOG in the spleen, it mainly distributed in the marginal zone and red pulp of the spleen. The CD11b immunofluorescence staining (Fig. 4e) showed that GOG local injection group had more activated macrophages in the white pulp and marginal zone, and the macrophages in red pulp also showed an high expression of CD11b protein marker. The different distribution of the $CD11b^{+}$ macrophages between the PBS and GOG injection groups illustrated that the marginal zone maybe was the important interaction site between the monocyte/macrophages and the graphene materials, which was conformed with the functional orientation of marginal zone as the innate immune response sites for bridging the innate and adaptive immune system [44]. All the above results illustrated that the GOG local application had an systemic promotive effect on the monocyte/macrophages activation in spleen, which might account for the observed regional acceleratory phenomenon (RAP) with accelerated bone remodeling in GOG local injection OTM model *in vivo*. Our this speculation about the promotive effect of the GOG induced monocyte/macrophages activation on bone remodeling was consistent to the previous report about the pivotal role of the monocyte/macrophage lineage cells in bone remodeling described by Yahara et al. [45]. Similar with our observation on the aggregation of GOG in spleen, the splenic capture and the biodegradation of graphene oxide (GO) nanosheet was also reported by Newman et al. recently [46]. Meanwhile, they also observed the distribution of GO in marginal zone of spleen. In our research, the GOG initiated innate immune response (monocyte/macrophages activation) in marginal zone of spleen had realized the remote regulation on alveolar bone remodeling, and this phenome would inspirate us to explore the underlying specific immunomodulatory mechanism and also provides us an promised immune-mediated strategy for the acceleration of bone remodeling.

3.3. The enhanced osteoclastogenesis of HSCs induced by co-culture with GOG stimulated BMSCs and the effects of PERK pathway on the functions of BMSCs

To investigate the effects of the GOG stimulated BMSCs on the osteoclastogenesis of HSCs, the co-culture system was designed for detection on the BMMs differentiation of HSCs with M-CSF induction and subsequent osteoclast differentiation of BMMs with M-CSF/RANKL combination induction. The schematic diagram (Fig. 5a) showed the induction process and the scheduled detections at different induction timepoints. The osteoclastogenesis of HSCs was initiated with the BMMs differentiation induced by 4 days of M-CSF stimulation. The FACS analysis on the proportion of the BMMs in HSCs after 4 days co-culture (Fig. 5b) showed that the GOG stimulated BMSCs could promote the BMMs differentiation of HSCs induced by M-CSF, which guaranteed a potential further differentiation of BMMs into mature osteoclast. For further detailed analysis on the mechanism in the osteoclastogenesis of BMMs, the intracellular calcium oscillation was detected after 2 days of M-CSF/RANKL combination induction to analyze the effects of the GOG stimulated BMSCs on calcium-signaling pathways, in which the changes of calcium oscillation could play a pivotal role in regulating the differentiation of BMMs into mature osteoclast [47]. The results (Fig. 5c) showed that the calcium oscillations of BMMs in the GOG treated group was significantly increased compared with the control groups, which would promote the further osteoclast differentiation of BMMs induced by M-CSF/RANKL combination induction. Meanwhile, the osteoblastic differentiation of BMSCs was also detected with ALP staining after 4 days of co-culture with HSCs induced by M-CSF and the results (Fig. 5d) showed an increased ALP activity in GOG stimulated BMSCs. Combining the detected results on the ROS activation and calcium ion concentration elevation (Fig. 3e and f) with the promoted osteoblastic differentiation of BMSCs, we deduce that the GOG initiated intracellular microenvironment change could regulate the osteoblastic differentiation of BMSCs under the co-culture with HSCs induced by M-CSF. Compared with our previous study on the osteoblastic differentiation of BMSCs under GOG stimulation in which the results just showed a slightly promotive effect of GOG on osteogenesis [36], the enhanced pro-osteogenic effect of GOG observed in this research might resulted from the co-culture with HSCs and the simultaneous M-CSF induction. Besides, the observed calcium concentration elevation in GOG stimulated BMSCs (Fig. 3f) might cause the increased calcium oscillation in BMMs through a potential intercellular transmissible ER stress regulatory mechanism that was described as a novel perspective on tumor intercellular communication by Jiang et al. [48]. Meanwhile, the intercellular transmission of hepatic ER stress in obesity was reported as an intercellular communication mechanism to disrupt systemic metabolism [49], which also indicated that the intercellular transmissible ER stress might function as an potential mechanism of the calcium oscillation translation and communication between the BMSCs and BMMs for the regulations on osteoblastogenesis and osteoclastogenesis. The reverse is true, too: the elevated calcium concentration might act as an intermediates to regulated the ER stress through the potential transmissible extracellular vesicles or direct diffusion pathway, which would set up a communication bridge between the co-culture cells for their inter-regulation on osteoblasto-/osteoclasto-genesis. So, the specific relationship of the intercellular ER stress and calcium oscillation transmissible pathways between the BMSCs and BMMs needs a comprehensive exploration to clarify the effects of GOG on the osteoblastogenesis and osteoclastogenesis in the co-culture system.

After 10 days of co-culture (4 days of M-CSF induction and 6 days of M-CSF/RANKL combination induction), the ARS staining of BMSCs and TRAP staining of the differentiated osteoclast progenitors (Fig. 5d) showed that the GOG stimulated group had the best osteoblastic differentiation of BMSCs and osteoclastic differentiation of HSCs. For verification on the regulative effect of PERK pathway that we proposed in the hypothesis (Fig. 3g) about the regulatory mechanism of the GOG stimulated BMSCs *in vitro*, the PERK inhibitor GSK2606414 was added in the GOG medium for blocking the PERK pathway and the GOG + GSK2606414 group showed an inhibited effect on the GOG promoted osteoblastic/osteoclastic differentiation (Fig. 5b, c and d). After 4 days co-culture with HSCs induced by M-CSF, the PCR analysis on the gene expression of GOG stimulated BMSCs (Fig. 5e) showed an increased expression of the osteoblastic genes including ALP, Runx2, Col1 and Ocn. Meanwhile, the gene expressions of RANKL was elevated and the OPG expression was decreased in GOG stimulated BMSCs resulting in an increased RANKL/OPG ratio, which indicated an potential promotive effects of GOG stimulated BMSCs on the osteoclastogenesis. Besides, the increased VEGF expression in the BMSCs co-cultured with HSCs indicated that the GOG stimulated interaction between the osteoblastic and osteoclastic progenitors had a promotive regulatory effect on angiogenesis, in which the promoted angiogenesis might further favor the recruitment of osteoblastic and osteoclastic progenitors.

About the osteoclastic differentiation of BMMs, the ER stress [28]

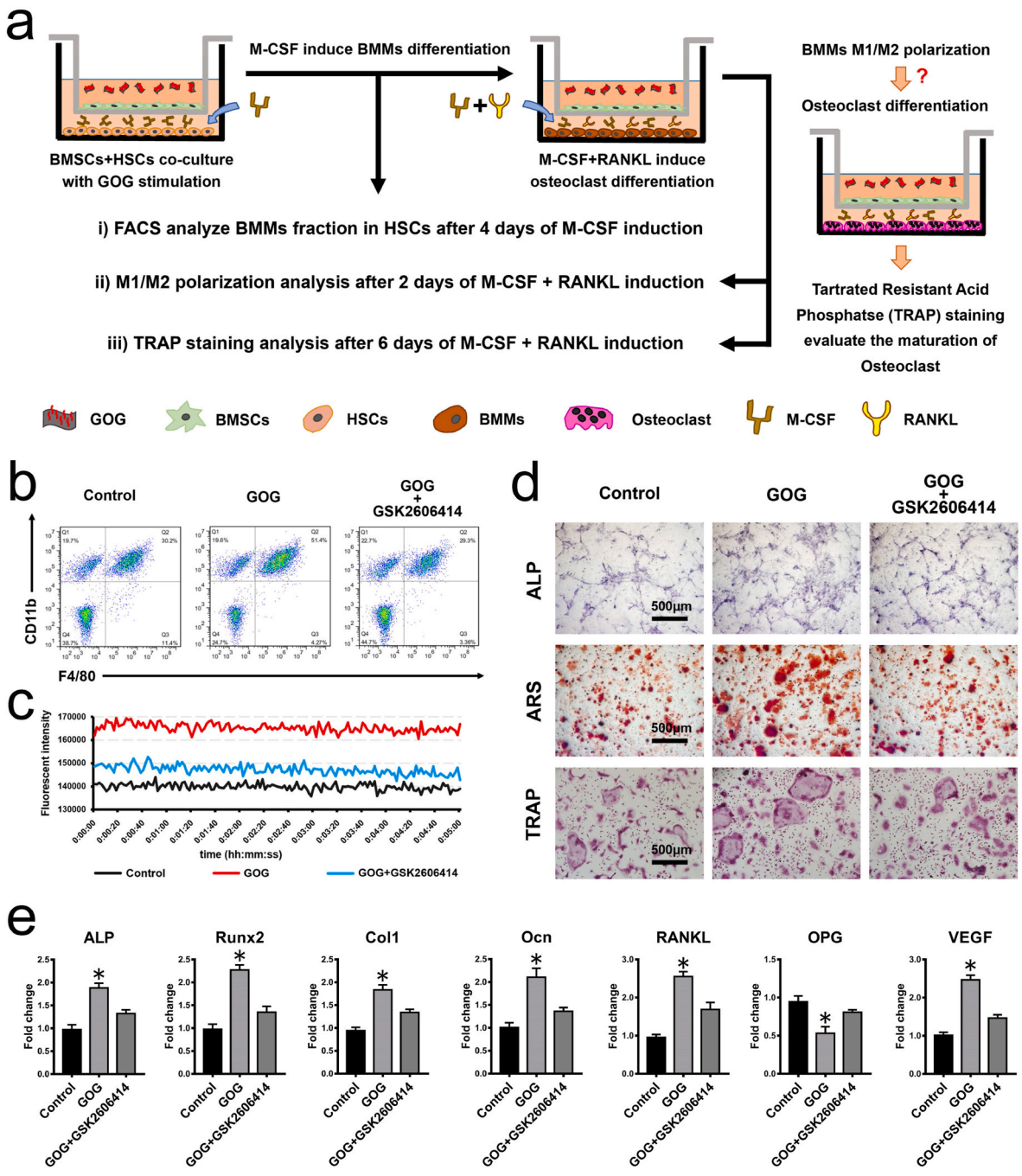

Fig. 5. The GOG stimulated BMSCs promoted the osteoclastogenesis of HSCs and the inhibited PERK pathway blocked the promotive effects of GOG on osteoblastic/osteoclastic differentiations. **(a)** The schematic diagram showed the designed induction procedure and scheduled detections at different timepoints. The HSCs were co-cultured with BMSCs in the transwell system for evaluation on the effects of GOG on osteoblastic and osteoclastic differentiations. The HSCs were cultured in the low chamber with 4 days of M-CSF (50 ng/mL) stimulus for inducing BMMs differentiation of HSCs. After 4 days M-CSF induction, the Flow cytometry analysis was conducted to evaluate the proportion of BMMs in total HSCs and the ALP staining was performed to evaluate the osteoblastic differentiation of BMSCs. The osteoclast differentiation medium containing 50 ng/mL M-CSF and 100 ng/mL RANKL was replaced at day 5 in the lower chamber for further analysis on osteoclastic differentiation of BMMs. In the subsequent induction of BMMs, the M1/M2 polarization was detected by M1/M2 specific markers (iNOS and arginase) immunofluorescent staining after 2 days of M-CSF + RANKL induction, and the calcium oscillation of BMMs was also detected after 2 days of M-CSF + RANKL induction. After 6 days of M-CSF + RANKL induction, the mature osteoclast differentiation from BMMs was verified by TRAP staining and the osteoblastic differentiation of BMSCs was evaluated by ARS staining. **(b)** The FACS analysis on the BMMs differentiation of HSCs, the $F4/80^{+}/CD11b^{+}$ proportion of the detected cells represented the differentiated BMMs from HSCs. **(c)** The calcium ion detection using the Fluo-4 AM probe, the fluorescent intensity represent the calcium concentration and the sequential detection were performed with 2 s interval for 5 min for analysis on calcium oscillation of BMMs after 2 days of M-CSF + RANKL induction. **(d)** The ALP and ARS stainings of the BMSCs showed the effects of GOG on osteoblastic differentiation of BMSCs after 4 days of M-CSF induction and 6 days of M-CSF/RANKL combination induction respectively. TRAP staining showed the osteoclastic differentiation of BMMs after 6 days of M-CSF/RANKL combination induction. bar: 500 μm. **(e)** The PCR analysis on the gene expression of BMSCs that were cultured with different media after 4 days co-culture with HSCs induced by M-CSF, the osteogenic genes such as ALP, Runx2, Col1 and Ocn, were up-regulated in the GOG stimulated group, the RANKL/OPG ratio and VEGF expression were also increased in GOG group. The PERK inhibitor GSK2606414 blocked the promotive effects of GOG on the expression of relevant genes in BMSCs. *$p < 0.05$ indicates significant difference compared to the control group.

and mesenchymal stem cells [50] were both reported to have a regulatory effect on the M1/M2 polarization of macrophages. Meanwhile, the inflammatory M1 macrophages had showed an inhibited effect on the RANKL induced osteoclastogenesis [27], and the M2 macrophages was reported to promote the functional osteoclast differentiation leading to bone loss in the postmenopausal osteoporosis [51]. Besides, the M2 macrophages was also reported to contribute to the osteogenesis and angiogenesis on the nanotubular TiO2 surfaces [52]. All the previous researches indicate that GOG initiated ER stress in BMSCs might has a regulatory effects on the M1/M2 polarization of BMMs to influence the osteoclastogenesis and the imbalanced M1/M2 polarization also might has a feedback regulation on the osteoblastogenesis. For further

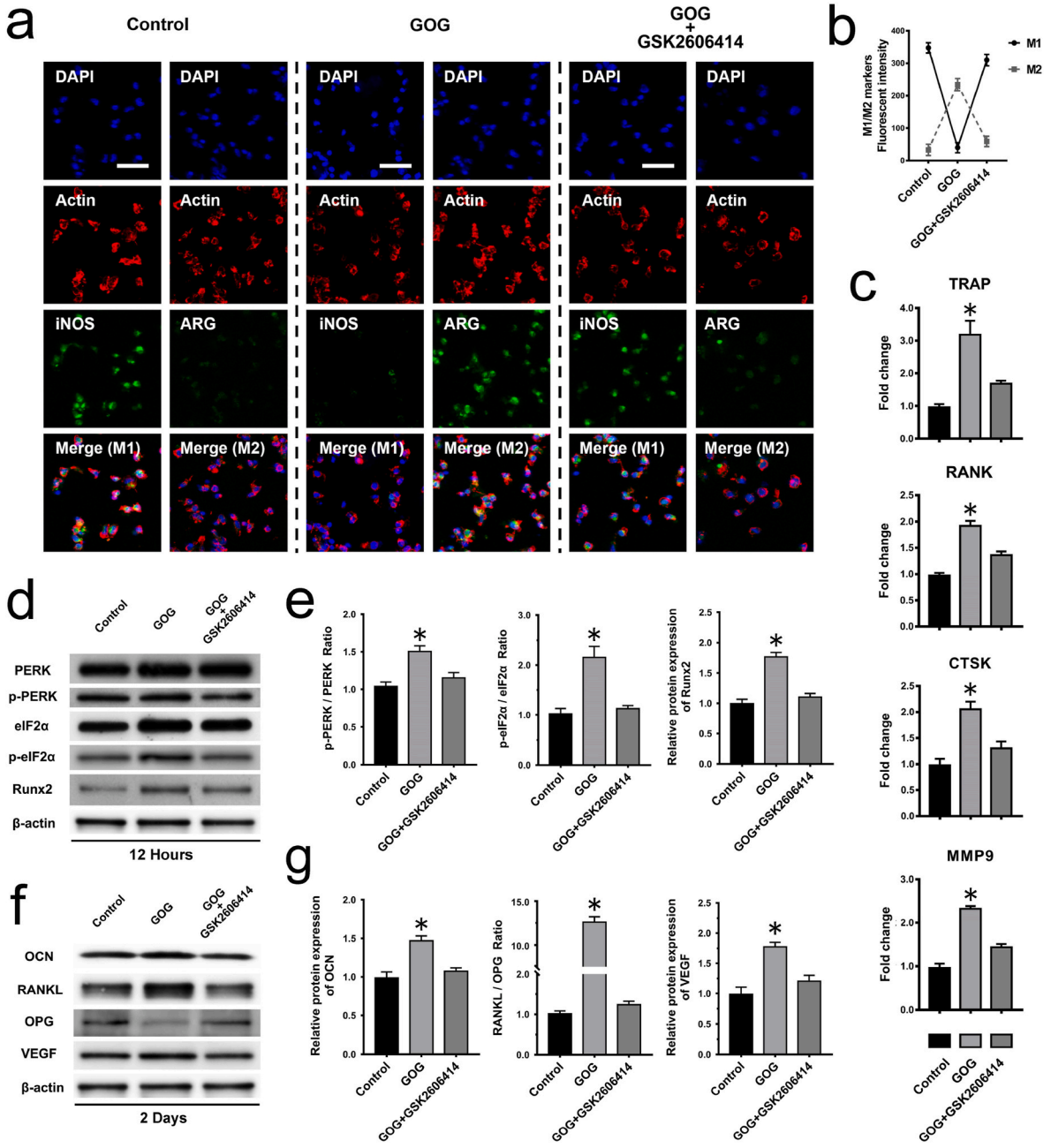

Fig. 6. The M2 polarization of BMMs was induced by GOG stimulated BMSCs and PERK pathway played an important role in the regulatory effects of GOG stimulated BMSCs. **(a)** The immunofluorescent staining on the M1/M2 specific markers of BMMs after 2 days of M-CSF/RANKL combination induction showed that GOG stimulation could promote the M2 polarization of BMMs, and GSK2606414 could block the regulatory effect of GOG stimulated BMSCs on macrophages M1/M2 polarization through inhibiting PERK pathway. bar: 50 μm. **(b)** The quantitative analysis on the fluorescent intensity of M1/M2 markers showed the diverse M1/M2 polarization of BMMs in different treatment groups. **(c)** After 6 days co-culture of BMSCs and BMMs with M-CSF/RANKL combination induction, the PCR analysis on the BMMs showed the increased gene expression of osteoclastic proteins, including TRAP, RANK, CTSK and MMP9. *$p < 0.05$ indicates significant difference compared to the control group. **(d)** The Western blot analysis of the PERK, p-PERK, eIF2α, p-eIF2α and Runx2 expression in BMSCs after 12 h co-culture with HSCs and M-CSF induction. **(e)** The quantitative analysis on the intensity of the WB bands showed the activation of PERK/eIF2α pathway and the increasement of the osteogenic differentiation transcription factor Runx2 in BMSCs. *$p < 0.05$ indicates significant difference compared to the control group. **(f)** The expression of OCN, RANKL, OPG and VEGF in BMSCs were detected by WB analysis after 2 days co-culture with BMMs and M-CSF/RANKL combination induction. **(g)** The quantitative analysis on the intensity of the WB bands showed the increased osteoblastic proteins and pro-osteoclastic/pro-angiogenic proteins in the GOG stimulated BMSCs. *$p < 0.05$ indicates significant difference compared to the control group.

evaluation on the M1/M2 polarization of BMMs after 2 days of M-CSF/RANKL combination induction during the osteoclastogenesis, the M1/M2 specific markers were stained to analysis the change of the BMMs polarization due to the co-culture with GOG stimulated BMSCs, and the results (Fig. 6a) illustrated that the more M2-type BMMs were detected in the GOG stimulated BMSCs co-culture group and the M1-type BMMs only accounted for a small proportion in the GOG group compared with control group. The quantitative analysis on the fluorescent intensity of the M1/M2 specific markers (Fig. 6b) showed that the co-culture with GOG stimulated BMSCs could promote the M2 polarization of BMMs. Combining with the TRAP staining results after 6 days of the M-CSF/RANKL induction, we concluded that the M2 polarization of BMMs favored the maturation of the osteoclast differentiation. The PCR analysis on the gene expression of the BMMs after 6 days of M-CSF/RANKL combination induction (Fig. 6c) showed that the expression of the osteoclastic genes were increased in the GOG group compared with the control group. All the results indicated that the co-culture with GOG stimulated BMSCs could promote the BMMs differentiation from HSCs and the M2 polarization of BMMs induced by GOG contributed to its further mature osteoclast differentiation.

The Western blot analysis (Fig. 6d and e) on the PERK and eIF2α in BMSCs after 12 h co-culture with HSCs and M-CSF stimulation showed that the expression of p-PERK and p-eIF2α were increased with the GOG stimulation and the PERK inhibitor GSK2606414 could attenuate the promotive effect of GOG on PERK resulting in the decreased expression of the relevant effector proteins located in the downstream of PERK pathway. After 12 h co-culture, the protein expression of Runx2 in BMSCs (Fig. 6d and e) was increased with the GOG stimulation and the GSK2606414 inhibited the Runx2 expression induced by GOG, which indicated that the PERK pathway played a pivotal role in regulating the osteoblastic differentiation of BMSCs. The OCN expression of the GOG stimulated BMSCs after 2 days BMMs co-culture with M-CSF/RANKL combination induction (Fig. 6f and g) showed the consistent detection pattern with Runx2, in which the GOG stimulation could increase the

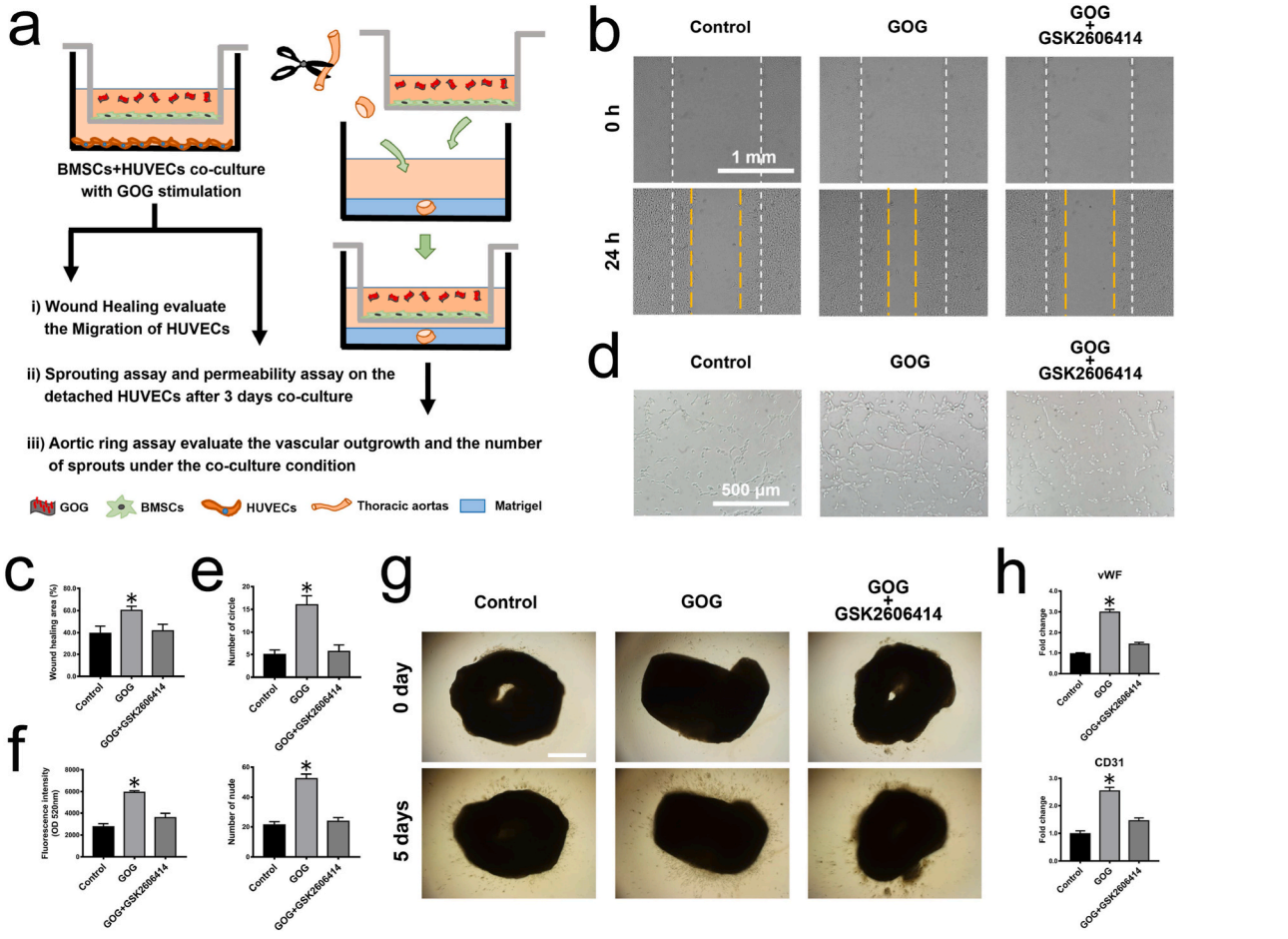

Fig. 7. The GOG stimulated BMSCs promoted the angiogenesis of HUVECs and the vascular outgrowth of aortic ring *in vitro*. **(a)** The schematic diagram showed the designed co-culture system for evaluation on the pro-angiogenic effect of GOG stimulated BMSCs. The upper chamber was seeded with BMSCs cultured with GOG medium, and the HUVECs were cultured in the lower chamber for further evaluation on its migration, sprouting and permeability abilities. The wound healing test was conducted directly with the HUVECs cultured in the lower chamber. For further analysis on the sprouting and vascular permeability of HUVECs, the HUVECs cultured in the lower chamber was detached by trypsin after 3 days co-culture with GOG stimulated BMSCs. The pretreated HUVECs was used for sprouting assay and permeability evaluation. The aortic rings was directly co-cultured with GOG stimulated BMSCs for 5 days to observe the number of new sprouts outgrowth from the aortic rings. **(b)** Images of the wound healing assay showed the migration of the HUVECs in different treated groups. bar: 1 mm. **(c)** The quantitative analysis on the migration distance of HUVECs. *$p < 0.05$ indicates significant difference compared to the control group. **(d)** The sprouting assay showed the HUVECs capillary tube formation capacity under different co-culture conditions. bar: 500 μm. **(e)** The quantitative analysis on the number of circle and node detected in the sprouting assay showed the pro-angiogenic effect of GOG stimulated BMSCs. *$p < 0.05$ indicates significant difference compared to the control group. **(f)** The quantitative analysis on the intensity of the penetrated FITC-dextran in the low chamber showed the permeability of the HUVECs in different groups. *$p < 0.05$ indicates significant difference compared to the control group. **(g)** The images of the aortic ring vascular outgrowth showed the more neogenesis of vascular vessels detected in the GOG stimulated BMSCs co-culture group. bar: 1 mm. **(h)** The PCR analysis on the HUVECs that had been co-cultured with GOG stimulated BMSCs for 3 days showed the increased gene expression of the vWF and CD31 angiogenic markers. *$p < 0.05$ indicates significant difference compared to the control group.

expression of OCN in BMSCs and the GSK2606414 blocked the promotive effect of GOG. Besides, the Western blot detection on RANKL, OPG and VEGF expressions in GOG stimulated BMSCs after 2 days BMMs co-culture with M-CSF/RANKL combination induction (Fig. 6f and g) showed the same expression trend with the PCR results of the GOG stimulated BMSCs after 4 days HSCs co-culture with M-CSF induction (Fig. 5e). The quantitative analysis of the Western blot (Fig. 6e and g) indicated the specific expression differences of the relevant protein factors among the different groups. All the results showed that the PERK pathway played a pivotal role in the regulatory effects of the GOG induced cellular stress due to the near location with the endoplasmic reticulum and mitochondria observed in our previous description (Fig. 3a–c), which would influence the bone remodeling in osteoblastogenesis, osteoclastogenesis and angiogenesis three aspects.

3.4. The angiogenesis of HUVECs and aortic ring assay were promoted by the GOG stimulated BMSCs

For detailed investigation on the pro-angiogenic effect of GOG stimulated BMSCs, we also designed the co-culture system of BMSCs

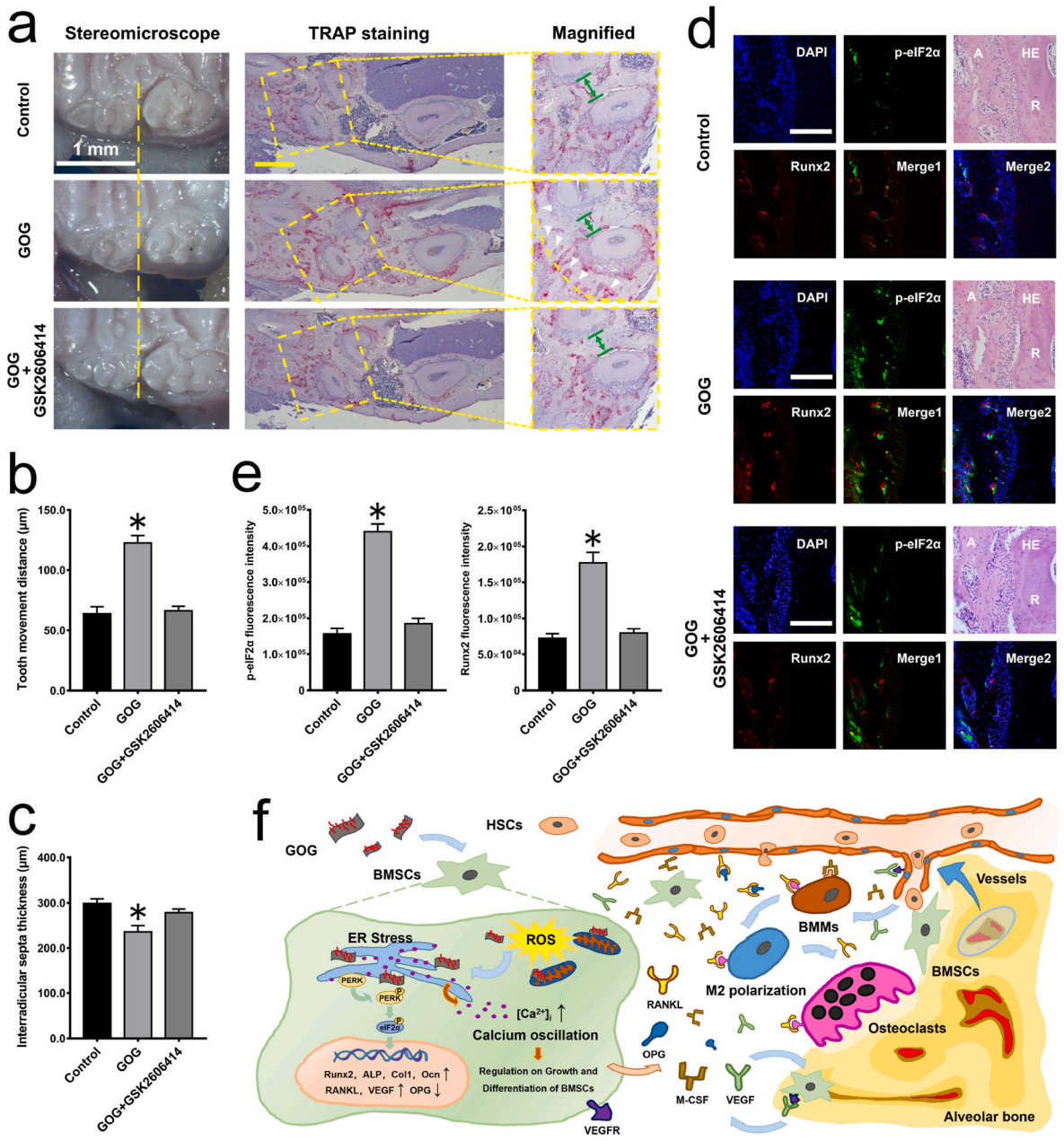

Fig. 8. The inhibited PERK pathway reversed the promotive effect of GOG on bone remodeling *in vivo*. **(a)** The observation on the tooth movement by stereomicroscopy and TRAP staining of the paraffin sections, white arrowheads indicated the blood vessels and the mature osteoclasts around them, the green lines in magnified fields enclosed the region of the interradicular septa. white bar: 1 mm, yellow bar: 500 μm. **(b)** The quantitative analysis on the tooth movements under different treatments, *p < 0.05 indicates significant difference compared to the control group. **(c)** The quantitative analysis on the interradicular septa thickness under different treatments, *p < 0.05 indicates significant difference compared to the control group. **(d)** The immunofluorescent staining of p-eIF2α (the effector protein of the PERK pathway) and Runx2 (osteogenic marker) showed the adjacent expression of the proteins in the tension side of the root during the orthodontic tooth movement, A: Alveolar bone, R: Root, bar: 100 μm. **(e)** The quantitative analysis on the fluorescent intensities of the p-eIF2α and Runx2 in the different treatment groups, *p < 0.05 indicates significant difference compared to the control group. **(f)** The schematic diagram showed the promotive mechanism of the GOG stimulated BMSCs on bone remodeling at osteoblastic, osteoclastic and angiogenic differentiations.

with HUVECs, and meanwhile further conducted aortic ring assay to mimic the angiogenesis *in vivo* (Fig. 7a). Migration assay of the co-cultured HUVECs in the lower chamber (Fig. 7b) showed a rapid wound healing in the GOG stimulated BMSCs co-culture group. The quantitative analysis on the wound healing area (Fig. 7c) showed that the HUVECs had about 50% increasement of migration distance in the GOG stimulated BMSCs co-culture group. The sprouting assay (Fig. 7d) illustrated that the capacity of the capillary tube formation was increased in the detached HUVECs that had been co-cultured 3 days with the GOG stimulated BMSCs, in which the vascular tubes formed in a more capillary-like network. The quantitative analysis (Fig. 7e) illustrated that the total numbers of the capillary-like circle and branch node point per field were increased more than 1.5 folds in the GOG stimulated BMSCs co-culture group compared with the control group. The permeability assay (Fig. 7f) detected more fluorescence intensity of the FITC-dextran in the low chamber of the transwell system in which the detached HUVECs were seeded in the upper chamber after 3 days co-culture with the GOG stimulated BMSCs (as described in Fig. 7a), which indicated that the co-cultured HUVECs with GOG stimulated BMSCs allowed more molecules in the upper chamber penetrate into the low chamber. Aortic ring assay (Fig. 7g) also showed the pro-angiogenic effects of the GOG stimulated BMSCs, the vascular outgrowth of rat aortic rings was more detected in the GOG stimulated BMSCs co-culture group. Besides, the GOG + GSK2606414 co-stimulated BMSCs co-culture group showed the inhibited effect on the pro-angiogenic function of the GOG stimulated BMSCs in the migration, sprouting, permeability detection assays of HUVEC and aortic ring assay, which showed the importance of the PERK pathway in the regulatory effects elicited by GOG stimulated BMSCs. The gene expression of the endothelial makers vWFs and CD31 in the HUVECs that were co-cultured 3 days with BMSCs (Fig. 7h), also showed an increasement in the GOG stimulated group and the co-stimulation of GOG + GSK2606414 could block the GOG stimulated pro-angiogenic effect. All the above results indicated that the GOG stimulated BMSCs had the promotive effects on the angiogenesis of HUVECs and also could promote the new capillary vessel outgrowth in the aortic ring assay, which proved the more active angiogenesis induced by GOG stimulated BMSCs *in vitro* and indicated the promised pro-angiogenic effect of GOG stimulation *in vivo*.

3.5. The promotive effect of GOG on tooth movement was inhibited by GSK2606414 with decreased bone remodeling in vivo

For verification on the pivotal role of the PERK pathway in the GOG stimulated bone remodeling *in vivo*, we further established the GOG + GSK2606414 co-injection OTM model to verify the function of PERK pathway in promoting bone remodeling. The tooth movement distance (Fig. 8a) was observed with the stereomicroscope and the quantitative analysis result (Fig. 8b) showed that the inhibited PERK pathway by GSK2606414 resulted in the deceleration of the tooth movement induced by GOG stimulation. The TRAP staining (Fig. 8a) also showed that the inhibited PERK pathway reversed the promotive effect of the GOG on tooth movement and bone remodeling. In the magnified field of TRAP staining, we could observe the promoted osteoclast-induced bone resorption and more blood vessels (the white arrowhead indicated the capillary blood vessels and functional osteoclast around them) in the GOG treated group compared with control group. Meanwhile, the thickness of interradicular septa (the sites indicated by green lines in Fig. 8a) in GOG group was decreased resulting from the active bone remodeling and the quantitative analysis on the thickness in different groups (Fig. 8c) showed that the GSK2606414 inhibited PERK pathway resulted in the increasement of the interradicular septa thickness. Besides, the number of mature osteoclast and new blood vessels around the bone remodeling were also reduced in the GOG + GSK2606414 group compared with GOG group, which showed the inhibited effect of PERK inhibitor GSK2606414 on GOG induced tooth movement acceleration. The immunofluorescent staining of p-eIF2α (the effector protein of the PERK pathway) and Runx2 in the tension side of the root showed the adjacent expression of p-eIF2α and Runx2 (Fig. 8d), in which the more activated PERK pathway (more detected p-eIF2α) elicited the high expression of Runx2 in the GOG injection group. The GSK2606414 inhibited the PERK activation with an decreased intensity of p-eIF2α resulting in the decreased expression of Runx2 in GOG + GSK2606414 injection group (Fig. 8e). The correlative expression pattern of the p-eIF2α and Runx2 corroborated the results about the PERK pathway *in vitro*. Combining with the observations on the bone resorption and new blood vessels formation, we could deduce that the mechanism of GOG *in vivo* was consistent with the verified mechanism that we had proved *in vitro*, in which the GOG stimulation can act on the pivotal regulatory cells BMSCs and arise the ER stress resulting in the UPR with activation of PERK pathway.

All the above results indicated that the GOG stimulated BMSCs played an important role in promoting bone remodeling at osteoblastic, osteoclastic and angiogenic differentiations (Fig. 8f). The verified effect of GOG stimulated BMSCs on regulating bone remodeling promised the local injection of GOG as a new choice of the methods that could induce RAP so as to accelerate the tooth movement. Meanwhile, the activated monocyte/macrophages in spleen by GOG and the pivotal regulatory role of BMSCs in bone remodeling gave us two extended exploration directions as the novel biomaterials application and mesenchymal stem cell regulatory biofunctions in promoting orthodontic tooth movement researches respectively. Our research showed that the novel GOG biomaterial has a good application prospect in accelerating orthodontic treatment.

4. Conclusion

Through the serial experiments *in vitro* and *in vivo*, we clarified the mechanism of GOG in promoting bone remodeling and the pivotal regulatory effects of GOG stimulated BMSCs in this phenomenon, which indicated the promised application of GOG in accelerating orthodontic tooth movement. The activated monocyte/macrophages in spleen and importance of the PERK pathway in accelerating tooth movement inspired us to explore more strategic choices of promoting orthodontic treatment, such as the systemic mobilization of the osteoclast progenitors, application of small molecule drugs to activate the PERK pathway or modulation on the biofunctions of BMSCs in promoting bone remodeling. Our research has extended the applications of novel biomaterials in accelerating orthodontic treatment and would inspire the researchers to explore more technical approaches for achieving more rapid and safe orthodontic treatment.

CRediT authorship contribution statement

Delong Jiao: Conceptualization, Data curation, Investigation, Methodology, Writing – original draft. **Jing Wang:** Methodology, Formal analysis. **Wenting Yu:** Formal analysis, Data curation. **Ke Zhang:** Methodology, Validation. **Ning Zhang:** Resources, Validation. **Lingyan Cao:** Methodology, Funding acquisition, Resources. **Xinquan Jiang:** Conceptualization, Funding acquisition, Project administration, Writing – review & editing, Supervision. **Yuxing Bai:** Conceptualization, Funding acquisition, Project administration, Writing – review & editing, Supervision.

Declaration of competing interest

We wish to draw the attention of the Editor to the following facts which may be considered as potential conflicts of interest and to significant financial contributions to this work.

We confirm that the manuscript has been read and approved by all named authors and that there are no other persons who satisfied the criteria for authorship but are not listed. We further confirm that the order of authors listed in the manuscript has been approved by all of us.

We confirm that we have given due consideration to the protection of intellectual property associated with this work and that there are no impediments to publication, including the timing of publication, with respect to intellectual property. In so doing we confirm that we have followed the regulations of our institutions concerning intellectual property.

We understand that the Corresponding Author is the sole contact for the Editorial process (including Editorial Manager and direct communications with the office). He is responsible for communicating with the other authors about progress, submissions of revisions and final approval of proofs. We confirm that we have provided a current, correct email address which is accessible by the Corresponding Author and which has been configured to accept email from Editor office.

Acknowledgments

This study was funded by China Postdoctoral Science Foundation (2021M692249), National Key R&D Program of China 2017YFC1104304 (YB), National Natural Science Foundation of China grant 82071144, Shanghai Rising-Star Program (21QA1405400) and Innovative research team of high-level local universities in Shanghai (SSMU-ZDCX20180900).

References

[1] R.M. Generson, J.M. Porter, A. Zell, G.T. Stratigos, Combined surgical and orthodontic management of anterior open bite using corticotomy, J. Oral Surg. (Am. Dent. Assoc.) 36 (3) (1978) 216–219, 1965.
[2] W.M. Wilcko, T. Wilcko, J.E. Bouquot, D.J. Ferguson, Rapid orthodontics with alveolar reshaping: two case reports of decrowding, Int. J. Periodontics Restor. Dent. 21 (1) (2001) 9–19.
[3] M. Nishimura, M. Chiba, T. Ohashi, M. Sato, Y. Shimizu, K. Igarashi, H. Mitani, Periodontal tissue activation by vibration: intermittent stimulation by resonance vibration accelerates experimental tooth movement in rats, Am. J. Orthod. Dentofacial Orthop. 133 (4) (2008) 572–583.
[4] K. Kawasaki, N. Shimizu, Effects of low-energy laser irradiation on bone remodeling during experimental tooth movement in rats, Laser Surg. Med. 26 (3) (2000) 282–291.
[5] S. Soma, M. Iwamoto, Y. Higuchi, K. Kurisu, Effects of continuous infusion of PTH on experimental tooth movement in rats, J. Bone Miner. Res. 14 (4) (1999) 546–554.
[6] M.A. Darendeliler, P.M. Sinclair, R.P. Kusy, The effects of samarium-cobalt magnets and pulsed electromagnetic fields on tooth movement, Am. J. Orthod. Dentofacial Orthop. 107 (6) (1995) 578–588.
[7] Z. Davidovitch, M.D. Finkelson, S. Steigman, J.L. Shanfeld, P.C. Montgomery, E. Korostoff, Electric currents, bone remodeling, and orthodontic tooth movement. II. Increase in rate of tooth movement and periodontal cyclic nucleotide levels by combined force and electric current, Am. J. Orthod. 77 (1) (1980) 33–47.
[8] H.M. Frost, Skeletal structural adaptations to mechanical usage (SATMU): 1. Redefining Wolff's law: the bone modeling problem, Anat. Rec. 226 (4) (1990) 403–413.
[9] D.J. Hadjidakis, Androulakis, II, bone remodeling, Ann. N. Y. Acad. Sci. 1092 (2006) 385–396.
[10] C. Verna, M. Dalstra, B. Melsen, The rate and the type of orthodontic tooth movement is influenced by bone turnover in a rat model, Eur. J. Orthod. 22 (4) (2000) 343–352.
[11] N. Udagawa, N. Takahashi, T. Akatsu, H. Tanaka, T. Sasaki, T. Nishihara, T. Koga, T.J. Martin, T. Suda, Origin of osteoclasts: mature monocytes and macrophages are capable of differentiating into osteoclasts under a suitable microenvironment prepared by bone marrow-derived stromal cells, Proc. Natl. Acad. Sci. U. S. A. 87 (18) (1990) 7260–7264.
[12] S. Theoleyre, Y. Wittrant, S.K. Tat, Y. Fortun, F. Redini, D. Heymann, The molecular triad OPG/RANK/RANKL: involvement in the orchestration of pathophysiological bone remodeling, Cytokine Growth Factor Rev. 15 (6) (2004) 457–475.
[13] T. Nakai, Y. Yoshimura, Y. Deyama, K. Suzuki, J. Iida, Mechanical stress up-regulates RANKL expression via the VEGF autocrine pathway in osteoblastic MC3T3-E1 cells, Mol. Med. Rep. 2 (2) (2009) 229–234.
[14] T.C. Dandajena, M.A. Ihnat, B. Disch, J. Thorpe, G.F. Currier, Hypoxia triggers a HIF-mediated differentiation of peripheral blood mononuclear cells into osteoclasts, Orthod. Craniofac. Res. 15 (1) (2012) 1–9.
[15] T. Nobuto, F. Suwa, T. Kono, Y. Hatakeyama, N. Honjou, T. Shirai, M. Mitsuyama, H. Imai, Microvascular response in the periosteum following mucoperiosteal flap surgery in dogs: 3-dimensional observation of an angiogenic process, J. Periodontol. 76 (8) (2005) 1339–1345.
[16] H. Glantschnig, J.E. Fisher, G. Wesolowski, G.A. Rodan, A.A. Reszka, M-CSF, TNFalpha and RANK ligand promote osteoclast survival by signaling through mTOR/S6 kinase, Cell Death Differ. 10 (10) (2003) 1165–1177.
[17] Z. Yao, L. Xing, C. Qin, E.M. Schwarz, B.F. Boyce, Osteoclast precursor interaction with bone matrix induces osteoclast formation directly by an interleukin-1-mediated autocrine mechanism, J. Biol. Chem. 283 (15) (2008) 9917–9924.
[18] K. Kayamori, K. Sakamoto, T. Nakashima, H. Takayanagi, K. Morita, K. Omura, S. T. Nguyen, Y. Miki, T. Iimura, A. Himeno, T. Akashi, H. Yamada-Okabe, E. Ogata, A. Yamaguchi, Roles of interleukin-6 and parathyroid hormone-related peptide in osteoclast formation associated with oral cancers: significance of interleukin-6 synthesized by stromal cells in response to cancer cells, Am. J. Pathol. 176 (2) (2010) 968–980.
[19] M. Schröder, R.J. Kaufman, ER stress and the unfolded protein response, Mutat. Res. Fund Mol. Mech. Mutagen 569 (1) (2005) 29–63.
[20] J. Lebeau, J.M. Saunders, V.W.R. Moraes, A. Madhavan, N. Madrazo, M. C. Anthony, R.L. Wiseman, The PERK arm of the unfolded protein response regulates mitochondrial morphology during acute endoplasmic reticulum stress, Cell Rep. 22 (11) (2018) 2827–2836.
[21] J. Guo, R. Ren, K. Sun, J. He, J. Shao, PERK signaling pathway in bone metabolism: friend or foe? Cell Prolif (2021), e13011.
[22] S.M. Chacko, S. Ahmed, K. Selvendiran, M.L. Kuppusamy, M. Khan, P. Kuppusamy, Hypoxic preconditioning induces the expression of prosurvival and proangiogenic markers in mesenchymal stem cells, American journal of physiology, Cell physiology 299 (6) (2010) C1562–C1570.
[23] M. Wang, W. Zhang, P. Crisostomo, T. Markel, K.K. Meldrum, X.Y. Fu, D. R. Meldrum, STAT3 mediates bone marrow mesenchymal stem cell VEGF production, J. Mol. Cell. Cardiol. 42 (6) (2007) 1009–1015.
[24] Y. Luo, Y. Wang, J.A. Poynter, M.C. Manukyan, J.L. Herrmann, A.M. Abarbanell, B. R. Weil, D.R. Meldrum, Pretreating mesenchymal stem cells with interleukin-1β and transforming growth factor-β synergistically increases vascular endothelial growth factor production and improves mesenchymal stem cell-mediated myocardial protection after acute ischemia, Surgery 151 (3) (2012) 353–363.
[25] J. Fiedler, F. Leucht, J. Waltenberger, C. Dehio, R.E. Brenner, VEGF-A and PlGF-1 stimulate chemotactic migration of human mesenchymal progenitor cells, Biochem. Biophys. Res. Commun. 334 (2) (2005) 561–568.
[26] D.E. Maridas, E. Rendina-Ruedy, P.T. Le, C.J. Rosen, Isolation, culture, and differentiation of bone marrow stromal cells and osteoclast progenitors from mice, JoVE : JoVE 131 (2018).
[27] T. Yamaguchi, A. Movila, S. Kataoka, W. Wisitrasameewong, M. Ruiz Torruella, M. Murakoshi, S. Murakami, T. Kawai, Proinflammatory M1 macrophages inhibit RANKL-induced osteoclastogenesis, Infect. Immun. 84 (10) (2016) 2802–2812.
[28] J. Oh, A.E. Riek, S. Weng, M. Petty, D. Kim, M. Colonna, M. Cella, C. Bernal-Mizrachi, Endoplasmic reticulum stress controls M2 macrophage differentiation and foam cell formation, J. Biol. Chem. 287 (15) (2012) 11629–11641.
[29] H. Takayanagi, S. Kim, T. Koga, H. Nishina, M. Isshiki, H. Yoshida, A. Saiura, M. Isobe, T. Yokochi, J. Inoue, E.F. Wagner, T.W. Mak, T. Kodama, T. Taniguchi, Induction and activation of the transcription factor NFATc1 (NFAT2) integrate RANKL signaling in terminal differentiation of osteoclasts, Dev. Cell 3 (6) (2002) 889–901.
[30] S. Patergnani, J.M. Suski, C. Agnoletto, A. Bononi, M. Bonora, E. De Marchi, C. Giorgi, S. Marchi, S. Missiroli, F. Poletti, A. Rimessi, J. Duszynski, M. R. Wieckowski, P. Pinton, Calcium signaling around mitochondria associated membranes (MAMs), cell communication and signaling, CCS 9 (2011) 19.
[31] M. Zayzafoon, Calcium/calmodulin signaling controls osteoblast growth and differentiation, J. Cell. Biochem. 97 (1) (2006) 56–70.
[32] S. Iyer, C. Melendez-Suchi, L. Han, G. Baldini, M. Almeida, R.L. Jilka, Elevation of the unfolded protein response increases RANKL expression, FASEB bioAdvances 2 (4) (2020) 207–218.
[33] T.P.D. Shareena, D. Mcshan, A.K. Dasmahapatra, P.B. Tchounwou, A review on graphene-based nanomaterials in biomedical applications and risks in environment and health, Nano-Micro Lett. 10 (3) (2018) 53.
[34] S. Mukherjee, P. Sriram, A.K. Barui, S.K. Nethi, V. Veeriah, S. Chatterjee, K. I. Suresh, C.R. Patra, Graphene oxides show angiogenic properties, Adv. Healthc. Mater. 4 (11) (2015) 1722–1732.
[35] S. Chakraborty, T. Ponrasu, S. Chandel, M. Dixit, V. Muthuvijayan, Reduced graphene oxide-loaded nanocomposite scaffolds for enhancing angiogenesis in tissue engineering applications, R. Soc. Open Sci. 5 (5) (2018) 172017.
[36] D. Jiao, L. Cao, Y. Liu, J. Wu, A. Zheng, X. Jiang, Synergistic osteogenesis of biocompatible reduced graphene oxide with methyl vanillate in BMSCs, ACS Biomater. Sci. Eng. 5 (4) (2019) 1920–1936.
[37] D. Jiao, A. Zheng, Y. Liu, X. Zhang, X. Wang, J. Wu, W. She, K. Lv, L. Cao, X. Jiang, Bidirectional differentiation of BMSCs induced by a biomimetic procallus based on a gelatin-reduced graphene oxide reinforced hydrogel for rapid bone regeneration, Bioact. Mater. 6 (7) (2021) 2011–2028.
[38] D. Jiao, J. Wang, W. Yu, N. Zhang, K. Zhang, Y. Bai, Gelatin reduced graphene oxide nanosheets as kartogenin nanocarrier induces rat ADSCs chondrogenic differentiation combining with autophagy modification, Materials 14 (5) (2021) 1053.
[39] Z. Zeng, Y. Li, Y. Pan, X. Lan, F. Song, J. Sun, K. Zhou, X. Liu, X. Ren, F. Wang, J. Hu, X. Zhu, W. Yang, W. Liao, G. Li, Y. Ding, L. Liang, Cancer-derived exosomal miR-25-3p promotes pre-metastatic niche formation by inducing vascular permeability and angiogenesis, Nat. Commun. 9 (1) (2018) 5395.
[40] G. Peng, M.F. Montenegro, C.N.M. Ntola, S. Vranic, K. Kostarelos, C. Vogt, M. S. Toprak, T. Duan, K. Leifer, L. Bräutigam, J.O. Lundberg, B. Fadeel, Nitric oxide-dependent biodegradation of graphene oxide reduces inflammation in the gastrointestinal tract, Nanoscale 12 (32) (2020) 16730–16737.
[41] E. Fessler, E.M. Eckl, S. Schmitt, I.A. Mancilla, M.F. Meyer-Bender, M. Hanf, J. Philippou-Massier, S. Krebs, H. Zischka, L.T. Jae, A pathway coordinated by

DELE1 relays mitochondrial stress to the cytosol, Nature 579 (7799) (2020) 433–437.
[42] R.E. Dolmetsch, R.S. Lewis, C.C. Goodnow, J.I. Healy, Differential activation of transcription factors induced by Ca2+ response amplitude and duration, Nature 386 (6627) (1997) 855–858.
[43] R.E. Dolmetsch, K. Xu, R.S. Lewis, Calcium oscillations increase the efficiency and specificity of gene expression, Nature 392 (6679) (1998) 933–936.
[44] J.M. den Haan, G. Kraal, Innate immune functions of macrophage subpopulations in the spleen, J. Innate Immun. 4 (5–6) (2012) 437–445.
[45] Y. Yahara, X. Ma, L. Gracia, B.A. Alman, Monocyte/macrophage lineage cells from fetal erythromyeloid progenitors orchestrate bone remodeling and repair, Front. Cell Dev. Biol. 9 (2021) 622035.
[46] L. Newman, D.A. Jasim, E. Prestat, N. Lozano, I. de Lazaro, Y. Nam, B.M. Assas, J. Pennock, S.J. Haigh, C. Bussy, K. Kostarelos, Splenic capture and in vivo intracellular biodegradation of biological-grade graphene oxide sheets, ACS Nano 14 (8) (2020) 10168–10186.
[47] H. Okada, K. Okabe, S. Tanaka, Finely-tuned calcium oscillations in osteoclast differentiation and bone resorption, Int. J. Mol. Sci. 22 (1) (2020).
[48] Z. Jiang, G. Zhang, L. Huang, Y. Yuan, C. Wu, Y. Li, Transmissible endoplasmic reticulum stress: a novel perspective on tumor immunity, Front. Cell Dev. Biol. 8 (2020) 846.
[49] A. Tirosh, G. Tuncman, E.S. Calay, M. Rathaus, I. Ron, A. Tirosh, A. Yalcin, Y. G. Lee, R. Livne, S. Ron, N. Minsky, A.P. Arruda, G.S. Hotamisligil, Intercellular transmission of hepatic ER stress in obesity disrupts systemic metabolism, Cell Metabol. 33 (2) (2021) 319–333, e6.
[50] D.I. Cho, M.R. Kim, H.Y. Jeong, H.C. Jeong, M.H. Jeong, S.H. Yoon, Y.S. Kim, Y. Ahn, Mesenchymal stem cells reciprocally regulate the M1/M2 balance in mouse bone marrow-derived macrophages, Exp. Mol. Med. 46 (1) (2014) e70.
[51] C. Dou, N. Ding, C. Zhao, T. Hou, F. Kang, Z. Cao, C. Liu, Y. Bai, Q. Dai, Q. Ma, F. Luo, J. Xu, S. Dong, Estrogen deficiency-mediated M2 macrophage osteoclastogenesis contributes to M1/M2 ratio alteration in ovariectomized osteoporotic mice, J. Bone Miner. Res. 33 (5) (2018) 899–908.
[52] J. Wang, S. Qian, X. Liu, L. Xu, X. Miao, Z. Xu, L. Cao, H. Wang, X. Jiang, M2 macrophages contribute to osteogenesis and angiogenesis on nanotubular TiO(2) surfaces, J. Mater. Chem. B 5 (18) (2017) 3364–3376.